

Understanding the Circulation Mechanism of Hydro Geothermal System in China

Roksana Bannya

Abstract

The present study focuses on hydro geochemical characteristics and circulation mechanism of deep geothermal water in study area. Isotopic and chemistry methods have been employed to enrich the study of the geothermal system. An emphasis is put on the estimation of the exchange temperature in the deep reservoir and the residence time of the geothermal waters. A total of 23 water samples were collected, which included 13 hot water samples and 10 cold water samples. The temperature range of cold water is between 25.2 to 28.5°C, and the pH values are nearly neutral. Hydrochemical type of cold waters is mainly HCO₃-Ca or HCO₃-Cl- Na-Ca. Hot water temperature ranges from 42.0 to 92.7°C, and the pH is weakly alkaline. There is a trend in the hydrochemical type of hot waters which shows a change from HCO₃-Cl-Na-Ca to Cl-Na type from inland to coastal areas within the studied area. We believe that Na-K-Ca geothermometer results are more accurate, and the average exchange temperature is estimated to be 171.9 °C. The hot water's circulation depths are between 105.4 to 2329.6 m. The cold water ratio in the mixed waters is in a range of 21% ~ 89%.

Keywords: geothermal water, exchange temperature, recharge source, deep-faults.

1. Introduction

Geothermal fluids have different chemical composition, which reflects their geological settings. These differences are associated with the source of the recharge waters and the contribution of magmatic or metamorphic gases and solutes^[2]. Williams, Reed^[3] defined a geothermal system as “any localized geological setting where portions of the Earth’s thermal energy may be extracted from natural or artificially induced circulating fluids transported to the point of use.” Geothermal systems are characterized by the temperature of the circulating fluids, geological setting of the area in which they are located, permeability and porosity of the host-rock, as well as their economic viability^[4]. The geothermal energy sector is earning more and more concerns by researchers as there is a growing demand for a new type of energy caused by a shortage of nonrenewable resources^[5]. Understanding processes occurring in the deep reservoir of the geothermal waters is key to sustainable development and utilization of the geothermal energy.

The coastal area of western Guangdong has deep faults zone which hosts abundant geothermal resources^[6], and qualitative evaluation on the formation and circulation of hot water resources is still needed. For this purpose, hydrochemical geothermometers may be used to infer the reservoir exchange temperature in a geothermal system. Hydrochemical geothermometers currently used are of types: including cation, silica, isotopes and gas geothermometers. To use a geothermometer, the solute or gas should have reached dissolution-equilibrium condition with the mineral in the host rock^[7, 8]. The chemical composition of geothermal fluid can give an insight into the extent of its interaction with the host-rock and is temperature dependent^[9]. This composition may change during the ascension of geothermal fluid as some gas may escape and solutes dissolve or precipitate. The mixing with shallow waters changes the chemical composition of the deep geothermal waters. Most of the geochemical processes, if not all, need to be taken into consideration to have an understanding of the circulation mechanism of fluids in a geothermal system^[2].

Guo, Gui^[10] found that the groundwater in the western part of Guangdong Province has a fast runoff and a considerable circulation depth during the process of formation of deep geothermal systems. Under the action of gravity, the external rainwater is deep-seeped through the bedrock fissure to form the groundwater which is continuously heated up during the runoff. This forms geothermal water of different temperature and fully react with the surrounding rock at high temperature^[11]. The time elapsed between the recharge and the sampling of the geothermal is a good indicator of the flowrate, migration process and the regeneration ability of a geothermal system^[12].

1.1 Target

Geothermal water resources are abundant in Guangdong province and are earning more concern by researchers^[13, 14], but there is not yet a qualitative evaluation on how to rationally develop and utilize these hot water resources. Groundwater in the western part of Guangdong Province has a fast runoff and a large circulation depth during the process of formation of deep geothermal systems^[6, 15]. Under the action of gravity, the external atmospheric precipitation is deep-seeped through the bedrock fissure, and the groundwater is continuously heated up during the runoff to form geothermal water of different temperature and fully react with the surrounding rock at high temperature. The

formation of complex hot water will inevitably occur in the process of strong carbonate minerals dissolution-precipitation reactions.

The aim of this study is to contribute to the understanding of circulation mechanisms of hydrothermal waters hosted by deep-faults by a qualitative evaluation of the exchange temperature in deep reservoirs using solute geothermometers, correction ^{14}C ages using different models, and the chemical and isotopic composition of the samples collected in coastal areas of Guangdong, south China.

1.2 Objectives

The overall objective is to give an insight into the understanding of underground circulation processes of geothermal waters hosted by deep faults for the accurate evaluation of Guangdong geothermal resources, sustainable development and usage prediction.

Specific objectives of the research are the followings:

To correct the study of ^{14}C age, eliminate the dead carbon, obtain the true age of geothermal water, and correctly evaluate the regeneration ability of geothermal water and hence acknowledge the origin of the underground water circulating in this coastal area.

To estimate the exchange temperature for deep faults hosted geothermal systems in Guangdong province by different hydrochemical geothermometers that include silica and cation geothermometers.

To contribute to the understanding of water-rock interactions in geothermal systems using different simulation computer programs.

1.3 Significance of the study

The present study focuses on a geothermal system hosted by deep faults of coastal Guangdong. Following are the main expected contributions:

The study will contribute to the estimation of exchange temperature between the host rock and the hosted water, which in most cases presents difficulties of direct measurements. Silica and cation geothermometers will be used and compared to the existing data to depict, which of them gives more accuracy.

To infer the elapsed time between recharge and discharge, which is very important information for it helps to know how much of the groundwater flow in and out of the system. Like this, the study will be useful for academics and researchers.

The results will contribute to the database on the Guangdong geothermal system hosted by deep-faults zone, which is crucial to its proper understanding and utilization.

1.4 Rationale, scope and context of the study

Geothermal energy as a new type of green energy, has attracted more and more attention. A large number of hot springs are exposed in the vicinity of the deep fault zone in western Guangdong, indicating that geothermal water resources are abundant in the region. Understanding the processes occurring in the hydrothermal system is the key to the sustainable development and utilization of geothermal energy. Geothermal water age is an important indicator of its flow direction, circulation speed and regeneration capability, which is an important scientific basis for the sustainable development and utilization of geothermal water. ^{14}C is one of the most important and reliable groundwater dating methods, widely used in groundwater dating from 1 to 35ka. Dissolved inorganic

carbon of the geothermal water contains ^{14}C depleted carbonates which dilute its ^{14}C content, which in this study will be recalibrated.

Apart from the ^{14}C age, which indicates the time elapsed between the recharge and discharge of the geothermal system, our study is entitled to determine the reservoir heat temperature using hydrochemical geothermometers. The chemical and isotopes characteristics of the sampled waters have been analyzed to better understand their origin and their reactions with the host rock.

The thesis is organized into five chapters. The first chapter gives a brief description and background, objectives and significance of the study. The second chapter delivers details on the current state of knowledge of the studies carried out on geothermal systems. An emphasis is put on solute geothermometers and ^{14}C ages as they are the main part of our study. Chapter three presents the research methods and materials used during experimentation. It emphasizes also on the sample collection and sample preservation. Chapter four concerns the study results and their discussions. The final, chapter five, gives concluding remarks of the study.

1.5 Study area

1.5.1 Geological setting of the study area

Guangdong is an important southern province that belongs to the Pearl River Delta of China. Geologically, Guangdong Province is located in the hinterland of Cathaysia Block along the SE margin of the South China Block^[16]. Different from most early Precambrian blocks, the Cathaysia Block is relatively young only with minor Paleoproterozoic rocks, although some Archean zircons have been reported. Except minor Paleoproterozoic rocks, several discrete episodes of granitic magmatism including Caledonian, Indosinian, early and late Yanshanian were widely distributed in this province, where the S-type or crustally remelting type granite is an important rock type^[17].

The study area is located in the western coastal area of Guangdong Province, Yangjiang - Maoming area, as shown in Figure 1. The range of coordinates is about $111^{\circ}00' \sim 112^{\circ}30'$ east longitude and $21^{\circ}20' \sim 22^{\circ}20'$ north latitude. It is an area of about 1000 km^2 including Gaozhou, Dianbai, Yangchun, Enping, Yangdong County and other areas. The strata in the area are exposed from the Sinian to the Quaternary discontinuity and are mainly composed of the Sinian-Cambrian clastic rocks. There are mudstone-Triassic clastic rocks and carbonate rocks in the north, and Quaternary sediments are distributed in the southeastern coastal areas, mainly by coastal and continental sediments. The intrusive rocks are mainly Cambrian - Silurian and Jurassic - Cretaceous granites. Some of the Cretaceous syenites and a variety of Triassic intrusions, including diorite, pyroxenite, gabbro and monzonite, are scattered. The magmatic ages span the Caledonian, Variscan-Indosinian and Yanshanian periods^[18, 19]. Also, these granite bodies are closely associated with several deep faults and various types of sedimentary basins^[20].

The faulted tectonic development in this area is dominated by the NE-trending deep fault zone and a few near-east-west faults, which are consistent with the whole tectonic system of Guangdong Province. The major deep faults are Wuchuan-Sihui deep fault zone (F1 and F2) and Enping-Xinfeng deep fault zone (F3 and F4), which are characterized by large scale and a long extension. The general trend of Enping-Xinfeng fault zone is 40° , experienced a long geological history and multi-stage magmatic activity, and it runs through the entire research area from north to south. The Wuchuan-Wuchuan fault zone has a general trend of $20\text{-}40^{\circ}$, which is formed in the late Caledonian

movement. It is a multi-cycle magmatic activity belt. There is a strong thermo-metamorphic belt along the deep fault zone^[21, 22]. The two major deep fault zones are distributed along the contact zone where clastic rock and magmatic rocks invade, and the hot springs are mainly distributed in the vicinity and the intersection of deep and large faults. These faults are large in scale and deep in cutting depth, providing migration channels for deep hot water flow. The fracturing of the strata is very intense, complex in its structure, and the water-bearing and water-conducting ability of the rock structure is better. This structural condition increases the probability of magma intrusion in the deep part of the earth, and upward heat transfer occurs, which leads to the formation of the deep- Geo-thermal zone^[21]. In the folds of the distribution, geothermal display is also more intensive, the hot water samples collected in this study are more distributed here. Therefore, where the magmatic rocks are in contact with the surrounding rocks and the vicinity of the deep and large fault zones and in the areas where the folds are distributed, the hot springs are exposed and linearly expelled along with these structural spreading directions^[23]

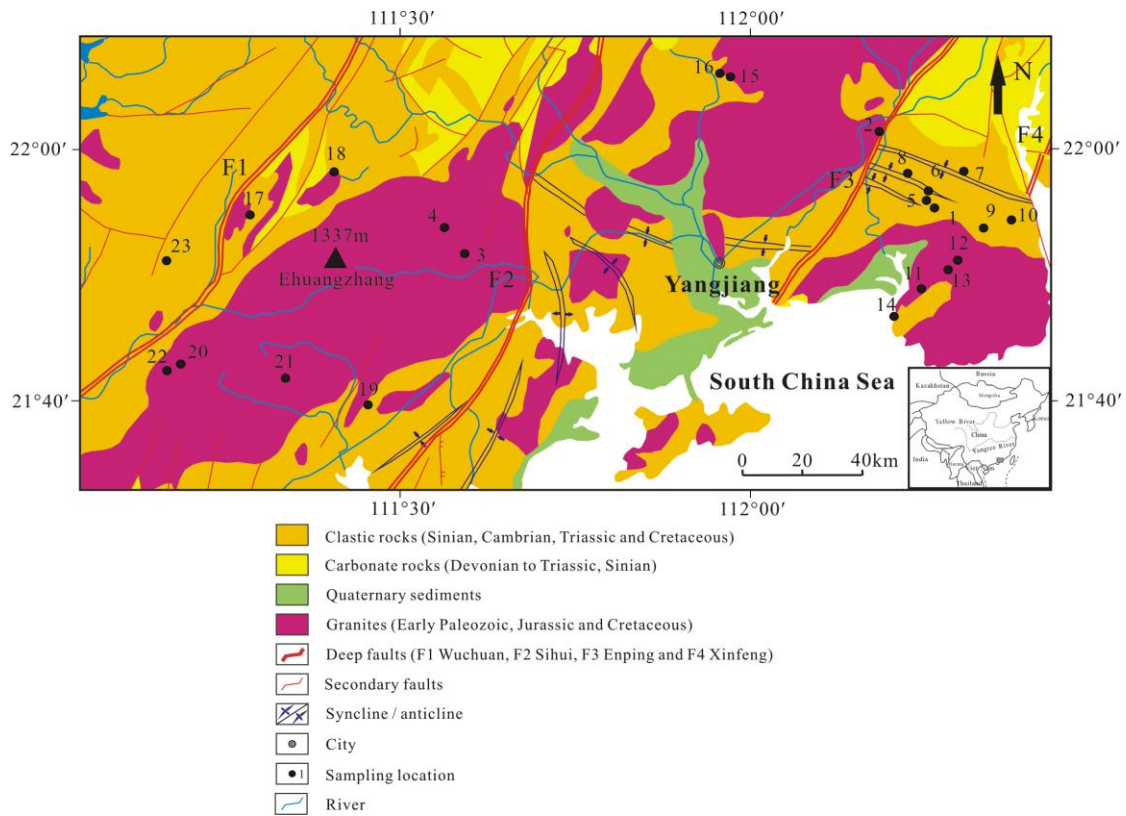


Fig. 1 Diagram of hydrogeological settings of the study area

1.5.2 Hydrogeology

The study area is composed of mountains and terraces with a relatively slow gradient. There are mountain ranges such as Huangshan, Yunwu Mountain and Ziluo Mountain. The elevation is within 800 ~ 1700m, and the relief is relatively small. As rain falls in this faulted zone, it penetrates porous sedimentary rocks, descends through it due to gravity and geochemically interacts with it. As it goes further beneath the surface, it gains heat from the primal heat of the Earth. A large thrust fault or crack is eventually encountered by this moving underground water^[24]. Therefore, the deep fault developed in

the study area, the fracture zone and the fissures generated during the formation of magmatic rocks all provide the channel for the runoff of underground hot water. The water of the studied area is mainly meteoric in origin.

In general, the main recharge forms of groundwater in the study area include rainfall infiltration recharge, river recharge, and the plain area may accept lateral recharge of mountain bedrock fissure water, infiltration recharge from irrigation water and so on. The groundwater discharge method include the spring water discharge, river discharge, artificial mining and transpiration.

2. Literature review

2.1 Characteristics of geothermal systems

Geothermal fields are distributed in different parts of the world under certain geological conditions and are gaining more attention as a new type of green energy. Every type of geothermal system has distinctive characteristics reflected in the chemical composition of the fluids and its potential applications^[25]. A heat source at a few kilometres depth is common to all of the geothermal systems, and it is this which sets water, present in the upper levels of the Earth's crust, into convection. Some of the geothermal resources find use in space heating applications such as greenhouse heating and urban heating schemes, but it is only the hotter systems ($>180^{\circ}\text{C}$) which can be used for electrical generation purposes through the production of steam^[26]. The water geochemistry is important in all steps of the exploration, evaluation, and production of a geothermal field since there is a need to understand the chemistry of the fluids for the development of a resource. The chemical composition of the fluids in a geothermal system carries information about its hydrology and the underground conditions in the reservoir rock^[27]. The chemistry of geothermal fluid and their characteristics are discussed shortly in this chapter. However, the specific aspects of geothermal chemistry will be discussed after a quick note to describe the geothermal system types.

A series of descriptive terms are used to classify differing geothermal fields. They are termed to be vapour or liquid dominated, low or high temperature, sedimentary or volcanic hosted etc. This section outlines the meaning of these and other descriptive classification terms we found in recent literature.

Reservoir equilibrium state: It is a basic criterion in differentiating geothermal systems and depends on the heat transfer and reservoir fluid circulation mechanism. Reservoir with a dynamic equilibrium are the ones in which water enters continuously^[28]. The water gains heat and ascends from the reservoir to the surface or underground permeable regions. Heat is transferred through the system by convection and circulation of the fluid. Geothermal systems in static equilibrium (also referred to as storage systems) have only minor, or no recharge to the reservoir and heat is transferred only by conduction^[26].

Fluid type: A reservoir fluid is termed to be liquid dominated when it is mainly composed of liquid water, and it is referred to as vapour-dominated in case the steam is its main component^[29]. Both steam and liquid water coexist in different proportions in most reservoirs^[30]. Most commonly, geothermal systems are liquid-dominated while those which discharge only steam are rare – the vapor dominated system best known are Larderello, Italy and The Geysers, USA^[31, 32].

Exchange temperature: The exchange temperature in geothermal reservoirs is an important factor as it is basic among the others in fluid chemistry and potential resource utilization. Low-temperature systems have a reservoir temperature less than 150°C, and they termed high-temperature systems when the temperature is great than that^[33]. However, the temperatures based classification is not rigid, and some geoscientists also use the term "intermediate" to indicate exchange temperatures between 120-180°C^[2, 34, 35].

Host rock: Chemical and physical interactions take place between the geothermal fluid and the hosting rock^[36]. Interactions between host rock and the contained fluid are determinant of the final composition of the geothermal waters and gases, knowing the host rocks is crucial for the confident application of hydrochemical geothermometers and predictions on potential scaling problems if the field is developed^[37, 38]. If the geology is poorly known, predictions on the sub-surface lithology from the water chemistry may be possible.

Heat source: The heat source for the system is a function of the geological or tectonic setting^[38, 39]. The invariably high-temperature systems are referred to as volcanogenic and their driving heat flux from magma. Heat does not, however, have to be supplied by magma, and a geothermal system can be generated in areas of tectonic activity. For example, heat may be supplied by the tectonic uplift of hot basement rocks, or water can be heated by unusually deep circulation created by folding of a permeable horizon or faulting. These are termed non-volcanogenic systems and include examples of both high and low-temperature reservoirs^[2, 40].

2.2 Formation of Geothermal waters

2.2.1 Origin of water and solutes

Geothermal water of a geothermal system can be derived from a number of sources. It may be meteoric water which descended depths of several kilometres through fractures and porous rock structures, or it can represent connate waters (water which was buried along with the host sediments)^[41]. Other sources of water in geothermal systems have been suggested; these include waters evolved in metamorphism (metamorphic waters) and from magmas (juvenile waters), but the importance of these sources of water is uncertain^[42].

The heat, water and solutes of geothermal systems were initially considered to be magmatic in origin. However, a demonstration on geothermal fluids proved their origin to be predominantly meteoric in the early 1960s and neat model was radically changed, and solutes could be derived from rock-water reactions^[2, 43]. The isotopic signature of the fluids studied by Craig^[44] demonstrated that geothermal fluids were meteoric in origin and could not be magmatic as their deuterium signature was similar to that of local meteoric water. All the solutes in geothermal fluids are mostly originated from fluid-host rock interactions^[45]. Rock-water reaction is considered as the important origin for many of the solutes, though some of them may also be originated from mixing with formation waters, magmatic brine or seawater^[46].

Geothermal fluids are mainly meteoric in origin, but the isotopic data are flexible to allow 5% to 10% of the fluids to originate from alternative sources, for instance,

magmatic brine^[47]. A small amount of the mixture of brine magma significantly affects the chemical properties of the final geothermal fluid, and the isotope determination can't preclude subsequent dilution of the magma contribution through meteoric water. However, the mass balance considerations for:

- water-rock ratios
- the chloride content of host rocks
- the concentration of chloride in waters from high-temperature systems
- the aerial extent of geothermal systems
- the duration of geothermal activity

Indicate that unrealistically large volume of rock would have to be leached over the lifetime of a geothermal system. A small but significant magmatic contribution to the geothermal fluid is therefore thought to be likely. Density differences would, however, preclude any intimate mixing between meteoric waters and a magmatic brine. If small pulses of magmatic brine did enter the geothermal convection cell then, while not detectable isotopically, they would make a major contribution to the solute composition^[48, 49]. Such would be at temperatures over 400°C and be rich in solutes such as Cl, SO₂ and CO₂. Although the extent to which mixing may occur is uncertain, recent analytical advances now make it possible to distinguish between the isotopes of chlorine and boron. A magmatic brine-meteoric water mixing model could be deduced from this isotopic information^[50, 51].

2.2.2 Evolution of geothermal waters

As discussed above, it is possible for fluid and solutes to be of additional sources. The evolution of geothermal fluids in dynamic, liquid-dominated systems can, in short, be stated as follows. Meteoric waters enter the crust through permeable zones and circulate to depths of up to around 5-7km^[52, 53]. As they descend, they are heated, react with the host rocks and rise by convection. Primary, these deep waters are chloride geothermal fluid in type from which all other types of geothermal waters are derived^[54]. At depth, the fluids typically contain 1000 - 10,000 mg/kg Cl at temperatures of about 350°C. The "soluble-group" elements are the first to be leached from the host rocks by the waters, followed by other elements which are controlled by temperature-dependent reactions^[2, 55]. These reactions change the primary mineralogy of the host rocks to a distinctive alteration assemblage characteristic of the fluid and its temperature. The fluids are retained within a permeable horizon forming a reservoir in which mineral-fluid equilibria, and a suite of secondary alteration minerals, are established^[56]. As the chloride fluids leave the reservoir and ascend to the surface, they may boil to create a two-phase (steam + liquid) boiling zone. The residual chloride water can discharge at the surface in hot springs or travel laterally to finally emerge many kilometers from the upflow zone^[57, 58]. The vapors from this boiling zone may migrate to the surface independently of the liquid phase and discharge as fumaroles. Alternatively, the vapors may dissolve in groundwater or condense in the cooler ground to form steam-heated, acid sulphate and/or bicarbonate waters^[59].

2.2 Age of geothermal waters in geothermal systems

Geothermal water dating is an effective means to determine the geothermal water recharge rate and infer the groundwater migration and flow model, which is very important for the accurate evaluation of groundwater resources sustainable development and usage prediction^[60]. ^{14}C dating is one of the most important and reliable methods for groundwater dating, which is widely used in groundwater dating from 1 to 35ka^[39, 61]. In essence, the ^{14}C age of groundwater is a measure of the age of Dissolved Inorganic Carbon (DIC) in groundwater, which is different from the true age of groundwater^[62]. The dissolved inorganic carbon in groundwater is multi-sourced and multi-genesis in its formation and evolution process. Different geochemical and geophysical processes contribute "dead carbon" to the DIC, leading to inaccurate age determination^[63]. According to the reaction process under different conditions, in recent years, a variety of calibration models have been developed for the correction of groundwater ^{14}C ages, such as Vogel, Tamers, Pearson, Gonfiantini, Mook and Fontes-Garnier models^[64-71]. However, due to the limitations of the conditions, the direct use of model calibration results are not reliable.

The growing shortage of nonrenewable resources has led to the rapid growth of the demand for new energy, geothermal as a new type of green energy earns more and more attention^[72, 73]. Understanding the processes occurring in the hydrothermal system is the key to the sustainable development and utilization of geothermal energy^[74]. Geothermal water age is an important indicator of its flow direction, circulation speed and regeneration ability^[47, 75]. As the geothermal water is different from the normal temperature groundwater, dissolved inorganic carbon which also contains the deep non-polar causes "dead carbon", the current ^{14}C age correction method can't solve its "dilution" problem, it needs to be recalibrated. If not corrected, the analysis of the study will be misleading^[76]. The development and utilization of geothermal resources require the country's huge investment and erroneous ^{14}C ages are likely to cause huge losses. At present, it is of great significance to correct the study of ^{14}C age, eliminate the dead carbon, obtain the true age of geothermal water, and correctly evaluate the regeneration ability of geothermal water.

Geothermal water resources are abundant in Guangdong province and are earning more concern by researchers^[13, 14], but there is not yet a qualitative evaluation on how to rationally develop and utilize these hot water resources. Groundwater in the western part of Guangdong Province has a fast runoff and a large circulation depth during the process of formation of deep geothermal systems^[6, 15]. Under the action of gravity, the external atmospheric precipitation is deep-seeped through the bedrock fissure, and the groundwater is continuously heated up during the runoff to form geothermal water of different temperature and fully react with the surrounding rock at high temperature. The formation of complex hot water will inevitably occur in the process of strong carbonate minerals dissolution-precipitation reactions, which in this study, through the age of western Guangdong the geothermal water, its regeneration ability can be inferred. The direct use of ^{14}C dating results will inevitably lead to greater error. In order to correctly understand the properties of geothermal water in western Guangdong, its development and utilization, the correction of ^{14}C age have a profound significance. The radiocarbon age of Guangdong geothermal waters has been discussed during the present study.

2.3 Hydrochemical geothermometers in estimating exchange temperature

The chemical composition of a geothermal fluid reflect largely its geological setting and differ from a geothermal system to another. The constituents of the geothermal fluids are dissolved gases and minerals. The difference in their chemical composition depends on the origin of the recharging waters and the contributed gases which may be of magmatic or metamorphic origin^[77]. Specific chemical equilibrium reactions are the basis of many of the geothermometers which can be used to good fluids and natural spring discharges. They provide valuable insight as to the nature of the system and “the choice and interpretation of the geothermometer data are the art of the exploration geochemist”^[78, 79].

The exchange temperature represents the heating capacity of the geothermal resources under the control of the fault structure^[80]. Knowledge of the deep reservoir temperature of a geothermal system has important significance in the effective utilization of the geothermal resources. Hydrochemical geothermometers can be used to infer the exchange temperature of deep geothermal system^[8]. Four types of such geothermometers are currently used, including cation geothermometer, silica geothermometer, isotope geothermometer and gas geothermometer. The use of these geothermometers is based on the fact that a solute or gas, used in geothermometer calculations, has reached a dissolution-equilibrium condition with the minerals of the host-rock in the reservoir^[7]. The chemical components of the solution ascending from the deep reservoir to the shallow layer can be changed by boiling process and degassing. When the hot water is mixed with the superficial cold water, the original dissolution equilibrium in the solution is often changed, leading to the dissolution or precipitation of some solutes in the solution^[81].

Care must be taken in applying geothermometers, otherwise the results and interpretations may give rise to serious errors. Therefore, the limitations of any geothermometer must be considered. The initial requirement is that samples are correctly taken, and the analyses are accurate. It is good practice to compare temperatures indicated by different geothermometers. Note that some geothermometers are empirical (e.g. Na-K-Ca, D'Amore and Panichi^[27] gas geothermometer), whereas others are based on thermodynamic properties (e.g. Na-K, K-Mg). As the factors controlling empirical geothermometers are not completely known, theoretical geothermometers may in some cases be more reliable.

3. Materials and methods

3.1 Samples collection and testing

In this study, twenty three samples were collected in the coastal area of western Guangdong, including surface water samples (river and sea water), hot spring water, borehole hot water and underground cold water (well water). One group of 10 cold water and another of 13 hot water samples have been chemically analyzed.

pH, conductivity (E_c) and salinity (TDS) were measured in situ by the 5-Star multi-parameter water quality analyzer (520M-01 model). The water samples to be geochemically analyzed were filtered, and a portion of the filtered sample was packed in a high density polyethylene bottle for anion analysis. Another portion was acidified with ultrapure nitric acid to $\text{pH} < 2$ for cation analysis. The analytical tests were carried out in the China University of Geosciences (Wuhan) Environmental studies' laboratory. The main anions (Cl^- , NO_3^- , SO_4^{2-} and F^-) were tested using the Dionex ion chromatograph model ICS1100. The main cationic component was tested using an inductively coupled plasma spectrometer (ICP-OES) (ICAP6300). The silica content was measured by spectrophotometry.

H, O and C stable isotopic compositions were measured with stable isotope ratio mass spectrometer (MAT253). The values of δD and $\delta^{18}\text{O}$ were expressed relative to SMOW and the precision was $\pm 0.2\%$. $\delta^{13}\text{C}$ values were expressed relative to PDB and the precision was $\pm 0.2\%$. The ^{14}C was determined radiometrically by liquid scintillation counting after conversion to benzene with the analytical error less than 0.5pMC. All the analysis work was done in the State Key Laboratory of Biogeology and Environmental Geology, China University of Geosciences (Wuhan).

3.2 Experimental equipment and software

The equipment in this experimental study has been mainly found in the State Key Laboratory of Environmental Studies, China University of Geosciences (Wuhan).

Table 1. Experimental equipment and software used

S/n	Equipment/software	Source
1	Water samples	Western Guangdong
2	Nitric acid analyzer (520M-01 model)	laboratory
3	Dionex ion chromatograph model ICS1100	laboratory
4	Spectrophotometer	laboratory
5	inductively coupled plasma spectrometer (ICP-OES) (ICAP6300)	laboratory
6	high density polyethylene bottle	laboratory
7	Glassware	laboratory
8	PHREEQCI program	Office computer
9	Isotope ratio mass spectrometer (MAT253)	Laboratory
10	5-Star multi-parameter water quality	laboratory

4. Results and discussions

4.1 Water chemistry and its isotopic characteristics

4.1.1 Water chemistry

Cold water had a temperature range of 25.2-28.5 °C while hot water temperature was of 42.0-92.7 °C. Cold water pH was neutral in the range of 6.10-7.85 (except 6 points outside). Hot water was weakly alkaline, its pH was in the range of 6.80-9.16 (except 17 points outside). The conductivity of hot water is obviously higher than that of cold water. The cold water samples' conductivity is less than 300 μ s / cm except that at sea water sampling point 14 which is 35300 μ s/cm, and the sampling point near the coastline is closer to the sampling point of the inland area rate.

The content of soluble SiO₂ in hot water changed greatly, it was in a range of 2.23-30.00 mg/L, which was lower than that of high temperature geothermal water. The F⁻ content of most hot water sampling points is above 10 mg/L, and in the range of 0-20.27 mg/L. In the studied area, the bedrock is dominated by granite, so it is possible to preserve the magmatic heat flow of the historical residuals, and the magma usually contains high fluorine content. Since fluorine and calcium are relatively similar in nature, the two are generally homologous. Ca²⁺ content of the underground hot water is high, so the F⁻ content is also high in the studied area. This shows that the material composition of groundwater mainly comes from the mineral composition in the surrounding rock, which is the result of the water-rock interaction. In addition to the nature of the rock, the temperature and pH value play an important role in controlling the fluorine content in groundwater. The fluoride content generally increases with the increase of groundwater temperature. Fluoride in the alkaline environment is not easy to precipitate, so the more alkaline groundwater is, the higher the fluoride content^[82]. As it can be seen from the results in Table 1, the fluoride content in the hot alkaline water is generally higher, while in neutral cold water is basically undetectable^[83].

Table 2. Sampling information and analysis results of major components of water samples

sample	water	T(°C)	pH	Ec(ms/cm)	TDS(mg/L)	K ⁺	Na ⁺	Ca ²⁺	Mg ²⁺	SO ₄ ²⁻	Cl ⁻	F ⁻	Br	HCO ₃ ⁻	SiO ₂
1	drill	92.7	7.19	5.17	2532	176.08	860.62	16.14	18.36	112.09	1576.82	2.05	6.26	44.80	51.62
2	drill	72.0	8.01	0.868	426	14.45	141.05	6.72	5.44	37.86	152.05	11.67	0.53	132.00	4.77
3	spring	42.0	9.16	0.2556	125	1.39	27.43	2.30	0.78	8.64	49.36	9.48	-	44.80	13.44
4	spring	63.7	8.64	0.2465	121	1.63	24.45	2.56	0.30	7.35	56.41	7.81	-	40.20	17.14
5	well	25.2	6.61	0.1965	-	1.27	4.69	33.30	1.24	3.97	5.06	-	-	127.60	-
6	well	28.0	4.95	0.0298	-	4.66	5.08	2.27	1.18	2.31	8.02	-	-	13.10	-
7	well	28.5	6.42	0.2499	-	3.37	4.76	35.42	4.44	14.30	7.58	-	-	127.60	-
8	well	25.5	6.18	0.2489	-	7.76	9.93	21.07	5.36	27.49	15.42	-	-	65.40	-
9	well	27.0	6.20	0.1993	-	1.51	6.05	20.94	4.33	11.19	10.00	-	-	42.50	-
10	well	25.0	7.17	0.0403	-	1.26	4.58	1.43	0.79	2.50	4.82	-	-	21.60	-
11	well	26.8	6.80	0.03	-	1.67	3.76	1.48	0.33	3.13	5.76	-	-	13.10	-
12	well	26.0	6.10	0.2908	-	2.12	14.26	15.35	6.02	13.41	18.72	-	-	94.90	-
13	river	28.5	6.95	0.0537	-	1.31	5.57	2.96	1.11	2.77	6.10	-	-	30.70	-
14	sea	26.0	7.85	35.3	-	4.95	131.5	5.21	15.12	33.36	284.92	-	1.02	121.00	-
15	spring	54.5	8.82	0.494	242	3.45	50.87	2.02	7.62	35.34	59.11	19.63	-	103.30	15.88
16	spring	55.4	8.74	0.512	250	3.63	51.33	2.36	9.07	41.94	65.05	20.20	-	102.20	17.73
17	spring	25.3	5.67	0.0402	20	0.83	0.84	4.33	0.24	4.32	7.42	0.40	-	19.50	4.87
18	spring	63.2	8.63	0.422	207	2.54	42.53	2.35	6.56	31.86	43.13	16.01	-	97.60	13.49
19	drill	79.2	6.8	13.62	6666	166.19	1362.73	1643.71	6.65	255.96	5026.07	0.00	26.85	33.30	18.12
20	spring	77.5	8.61	0.379	186	2.89	36.65	2.14	2.14	13.69	61.02	13.49	-	89.50	22.79
21	spring	53.5	8.88	0.928	453	9.15	139.89	20.53	0.01	22.75	253.98	6.40	1.28	31.00	11.88
22	spring	45.0	8.96	0.405	198	2.44	41.25	2.96	5.04	27.27	55.67	19.74	-	97.60	19.68
23	spring	42.2	8.92	0.413	202	2.92	42.14	2.99	5.42	28.91	72.38	20.27	-	82.60	22.31

The three-linear diagram of the water sample is made according to the main ion content of cold and hot water and the relative concentration of the chemical components in the water samples, as shown in Fig. 2^[84]. In the figure, all the sampling points in the lower right triangle gather at the lower boundary of the triangle, showing that the anion content in geothermal water is mainly HCO_3^- and Cl^- while the content of SO_4^{2-} is relatively low. SO_4^{2-} content gradually increased with the water-rock interaction. The sampling points in the lower left triangle are also gathered in the lower boundary, reflecting that the groundwater cations are mainly Na^+ and Ca^{2+} , while the content of Mg^{2+} is relatively low.

Geochemically, the groundwater type can be roughly divided into four blocks:

A、A region of the HCO_3^- and Ca^{2+} ions based groundwater, found in cold water sampling points. The bedrock in this area is mainly granite, and the chemical properties of cold water show the mineral characteristics of the surrounding rocks.

B、A region that includes HCO_3^- , Cl^- anions and Ca^{2+} , Na^+ cations. It has hot water and cold water and is characterized by transitional water chemistry.

C、The hot water sampling points 17; 19 and the cold water sampling point 6 form a region where the anion is Cl^- , the cations being Ca^{2+} and Na^+ .

D、Seawater sampling point 14, a region for the Cl^- anion and Na^+ cation. In addition to the seawater sampling point 14, higher Cl^- may be formed by the influence of seawater, and it is also possible that the geothermal water fully reacts with the granite at high temperature during the runoff process forming a highly salty water.

In short, the hot water shows a trend of transition from $\text{HCO}_3^- \cdot \text{Cl}^- \cdot \text{Ca} \cdot \text{Na}$ type to $\text{Cl}^- \cdot \text{Na}$ type from inland to coastal areas.

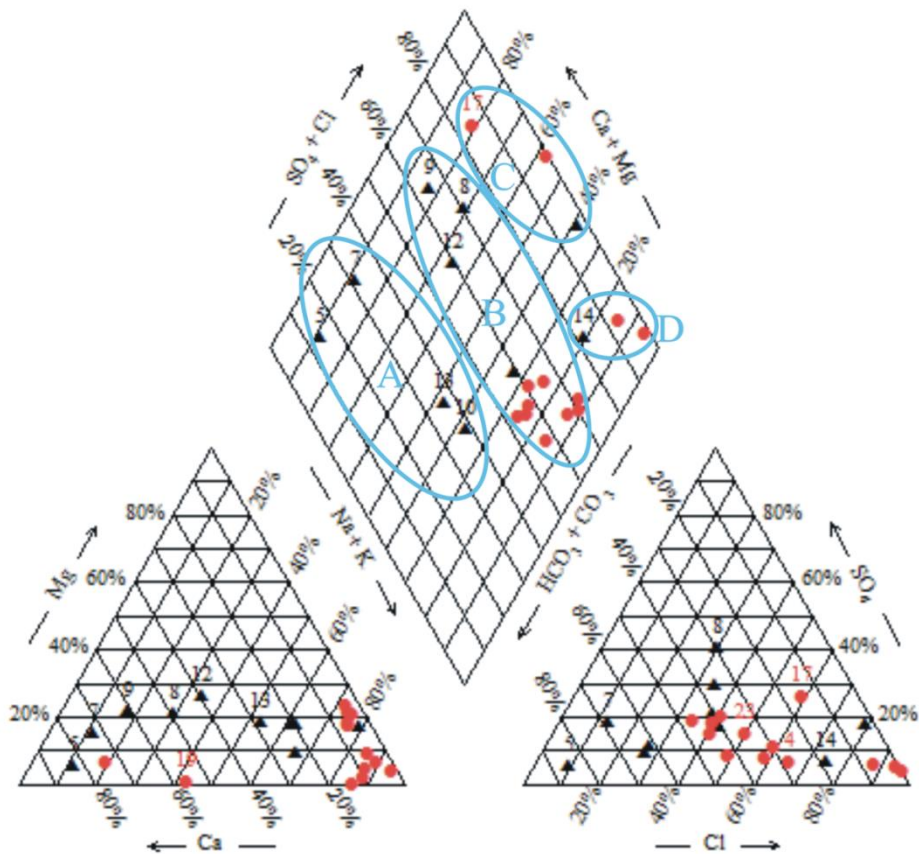


Fig. 2 The piper chart for water samples. The dots represent the hot water samples, the triangles represent the cold water samples.

4.1.2 Hydrogen and oxygen isotope characteristics

Different types of groundwater in different regions show different the δD and $\delta^{18}O$ values. In the δD - $\delta^{18}O$ scatter plot of the hot water, it can be seen that the underground hot water is located near the precipitation line in the coastal areas of western Guangdong, indicating that the groundwater is mainly supplied by the precipitation. The results show that different water bodies have different hydrogen and oxygen isotopic characteristics. Hydrogen and oxygen isotope measurements were performed on 13 hot water samples collected in the study area. The $\delta^{18}O$ value of the geothermal water was $-5.50\text{‰} \sim -7.34\text{‰}$ while that of δD was $-40.0\text{‰} \sim -51.4\text{‰}$, the measurement accuracy being $\pm 2\text{‰}$ and $\pm 0.2\text{‰}$ for δD and $\delta^{18}O$ respectively. The results of the test are compared with the V-SMOW standard, expressed as a symbol δ . According to the location of the sampling point, the characteristic values of hydrogen and oxygen isotope of hot water are shown to be increasing from inland to coastal areas.

In 1961, Craig summed up δD and $\delta^{18}O$ values of atmospheric precipitation in various regions of the world, and pointed out that δD was linearly related to $\delta^{18}O$ in the meteoric water and fitted with a global atmospheric precipitation fractional line. The equation was $\delta D = 8\delta^{18}O + 10$ ^[43, 85]. Figure 3 is a plot of relationship between the calculated δD and $\delta^{18}O$ values, for the hot water sampling point. In the figure, the solid line is the global precipitation line, and the long dashed line is the local precipitation line. The local atmospheric precipitation line used in this paper is Guangzhou atmospheric

precipitation line, whose equation is $\delta D = 8.1\delta^{18}O + 11.4$. The short dashed line is the atmospheric precipitation fractionation line in china and the equation is $\delta D = 7.44\delta^{18}O + 1.61$.

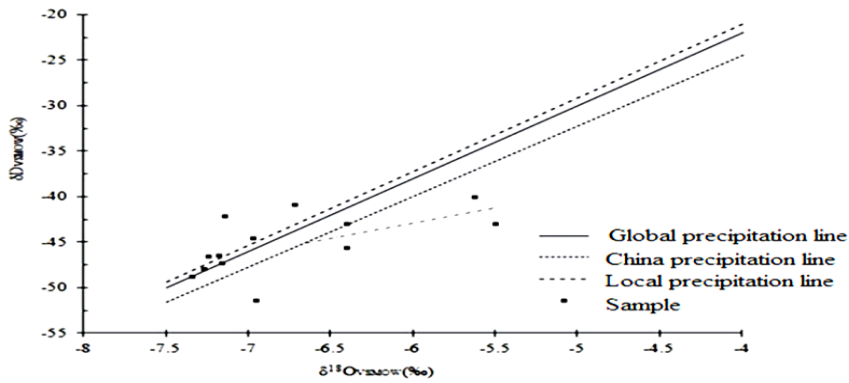


Fig. 3 Relationship between δD and $\delta^{18}O$ of geothermal water in the coastal area of western Guangdong.

As it can be seen from Figure 1, the geothermal water sampling points in the area are scattered. Most of the hot water gathered in the lower left of the precipitation line, indicating that hot water are meteoric in origin. The $\delta^{18}O$ value of the hot water point has obvious "drift" to the right, which may be due to the higher temperature of the geothermal water, the circulation depth, the hot water along the deep fault in the process of rising, the reaction of the surrounding rock is intense, and the isotopic exchange reaction takes place. When the water-soluble filter wall rock ^{18}O content of the surrounding rock is high, the hot water ^{18}O content also becomes larger. The δD value of geothermal water is less affected by this isotope exchange because the hydrogen content in the surrounding rock is very low^[86]. The four points of the line and the evaporation line is similar to that of hot water may also be caused by evaporation of hydrogen and oxygen isotope abundance values increase. Since not all of the hot water drift occurred, only one of the 1,4,19 and 21 points displayed oxygen drift, indicating that the geothermal water may be subject to mixing with shallow water.

4.1.3 Br- / Cl- ratio characteristics

Chloride (Cl) and bromide (Br) ions are ubiquitous solutes in all natural water. The first is a major component, the latter a minor one. The major reservoir of water (the ocean) has relatively uniform Cl and Br concentrations and their Cl/Br molar ratio is around 655 ± 4 ^[87, 88], although other authors report slightly higher or lower ratios, which may be explained by analytical accuracy and local effects.

Cl and Br ions dissolved in natural water are tracers close to the ideal conservative behavior due to their hydrophilic character and small ionic size^[89, 90]. Neither of them take part in significant ion exchange reactions at low temperatures, nor are they adsorbed onto mineral surfaces, and as they are so highly soluble, they only form minerals during extreme evaporation conditions when halite starts to precipitate^[91-93]. This means that the physical processes taking place in soil (dilution, evaporation, transpiration, mixtures, etc.) can change the absolute concentrations, but do not significantly modify the Cl/Br ratio of not-too-saline groundwater.

The Br^-/Cl^- ratio is an important tool for estimating the source of groundwater salinity, especially in distinguishing between continental evaporation and marine sources aspect. In 1996, Edmund established the Br^-/Cl^- logarithmic relationship with respect to seawater, rainfall and unsaturated zone aquifers by studying the Br^- and Cl^- levels in typical UK and all major aquifer streamlines. In the figure, the Br^-/Cl^- ratios are 1×10^{-2} , 4.47×10^{-3} and 1×10^{-3} , respectively. Where the Br^-/Cl^- ratio of 3.47×10^{-3} represents the sea water dilution line, where the point at or near the line is considered to be from sea water or residual marine source; a line with a ratio of 1×10^{-3} For the salt-dissolving line, the point above the line indicates that the chloride from the non-marine source is added or mixed[94].

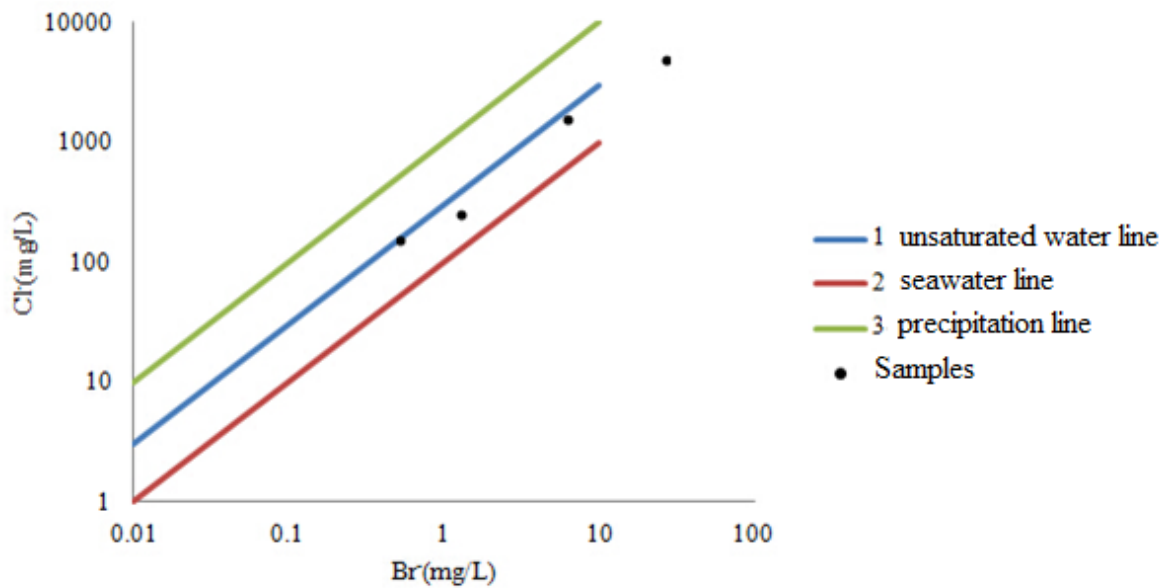


Fig. 4 Br^-/Cl^- logarithmic graph of hot water in the study area

The Br^-/Cl^- value can be calculated from the Br^- and Cl^- content of the hot water tested. In the measured data, the Br^- content of most hot water is closer to the points 1, 2, 19 and 21, indicating that these hot water points are derived from precipitation. This conclusion is consistent with the analysis of the characteristic values of hydrogen and oxygen isotopes. The Br^-/Cl^- ratio results for points 1, 2, 19 and 21 were calculated as 3.97×10^{-3} , 3.45×10^{-3} , 5.34×10^{-3} and 5.05×10^{-3} , respectively. Projected to the Br^-/Cl^- logarithmic diagram (Figure 4), it can be seen that these sampling points are distributed near the unsaturated zone, indicating the mixing of seawater. And these four points are located in the vicinity of the coastline, it can be inferred that the study area inland hot water are derived from atmospheric precipitation, and because of proximity to the coastline of these sampling points, there is mixing with seawater.

4.2 Hot and cold water mixing ratio

From the previous analysis, we can see that the geothermal water in the study area is mixed with the shallow cold water as the temperature decreases and the ionic components of the hot water is changed during the process of moving upwards along the deep faults. There are several ways to calculate the mixing ratio of hot and cold water, including tritium content calculation method, thermometer method, PHREEQCI software

simulation and hydrogen and oxygen isotope value calculation method. Hydrogen isotope calculation is used in this work^[95, 96].

When there is mixing of cold water with hot water, linear relationship between the mixed water SO_4^{2-} content and temperature T value, Cl^- content and temperature T, Cl^- and SiO_2 is observed^[95], as shown in Figure 5,6, and 7. It can be seen that there is a positive correlation between SO_4^{2-} content and temperature T value, Cl^- content and temperature T, and the linear relationship between Cl^- and SiO_2 is the most obvious. This further proves that the hot water in the study area is mixed with the shallow cold water.

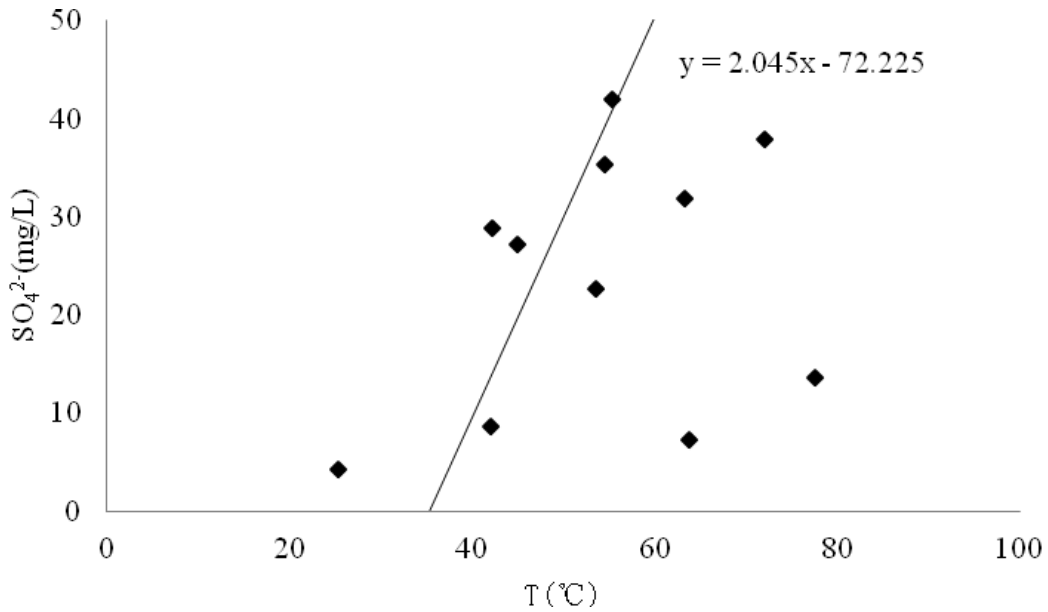


Fig. 5. SO_4^{2-} content in the hot water samples and temperature T relationship diagram

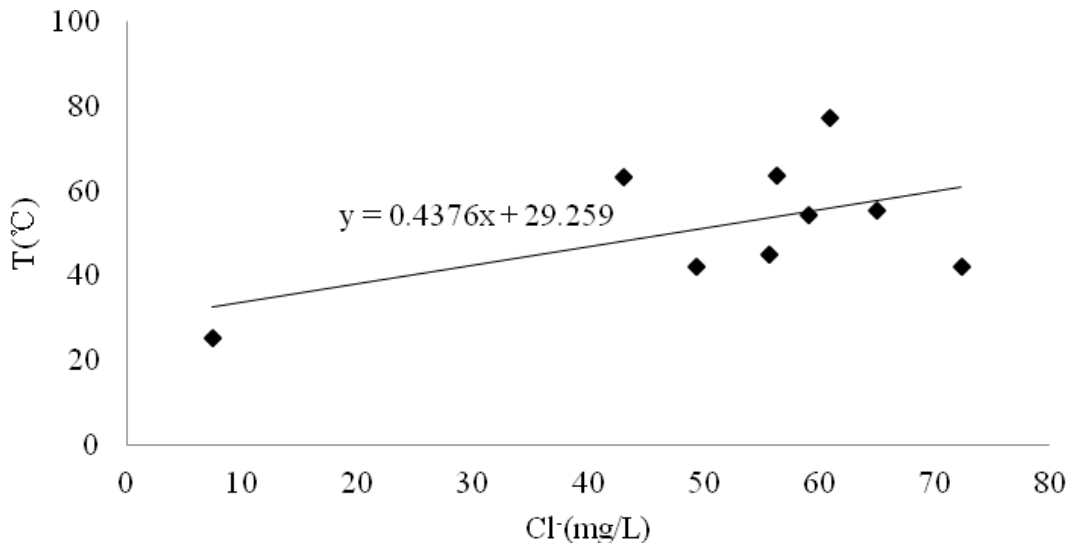


Fig. 6. The relationship between Cl^- and T in hot water samples

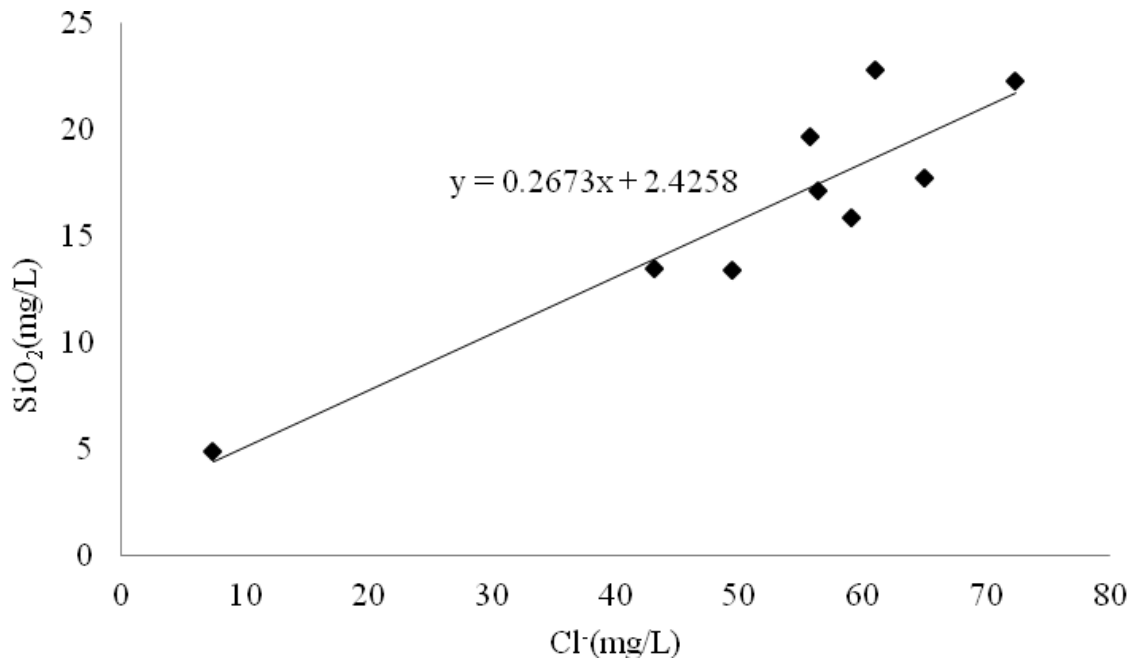


Fig. 7. Relationship between Cl⁻ content and SiO₂ value in hot water samples

The mixing ratio between cold water and hot water is related to the hydrogen and oxygen isotopic characteristics of mixed water and can be calculated from the δD value of mixed water. Among them, the formula is as follows^[97]:

$$\text{Cold water / hot water} = (\delta \text{ hot} - \delta \text{ mixed}) / (\delta \text{ mixed} - \delta \text{ cold})$$

$$\text{Cold water ratio} = (\delta \text{ hot} - \delta \text{ mixed}) / (\delta \text{ hot} - \delta \text{ cold})$$

At sampling point 20 where δD value is minimal with a value of -51.4 is took as the reference for the calculation of the mixing ratio of hot water and cold water, we attribute 0 as the mixing ratio at point 20. According to the data, the values of δD and δ¹⁸O in the underground cold water of western Guangdong were between -49.0 ‰ ~ -38.6 ‰ and -7.4 ‰ ~ -5.9 ‰, respectively, with the mean values of -44.83 ‰ and -6.59 ‰, respectively. The δD and δ¹⁸O values of surface water were between -41.0 ‰ and -45.0 ‰ and -5.6 ‰ to -6.6 ‰, respectively, and the mean values were -43.0 ‰ and -6.1 ‰, respectively. According to the results in Table 3, it can be seen that the mixing ratio of shallow cold water in mixed hot water is 21% ~ 89%. From the calculated mixing ratio, it can be seen that the positions of points 1, 4, 19 and 20 with higher mixing ratio of cold water are close to the coastal area, which is consistent with the Br⁻/Cl⁻ ratio results.

Table 3. Cold and hot water mixing ratio calculation results

Sample no.	δD _{VSMOW} (‰)	Cold water content (%)	Sample no.	δD _{VSMOW} (‰)	Cold water content (%)
1	-43.0	66%	18	-44.5	54%
2	-46.5	38%	19	-43.0	66%
3	-46.4	39%	20	-51.4	0
4	-40.0	89%	21	-45.6	45%
15	-48.7	21%	22	-40.8	83%
16	-47.9	27%	23	-42.1	73%

17	-47.3	32%
----	-------	-----

4.3 Exchange temperature calculation by hydrochemical geothermometers

Most of the chemical reactions are temperature dependent in a geothermal system^[98]. Geothermometry is a simple and effective method for estimating exchange temperature at the deep level^[99]. In geothermal systems, hot water migration process from deep to shallow levels is accompanied by a variety of mineral phase dissolution and precipitation reaction. Chemical geothermometers are based on temperature-dependent, water-rock reactions that control the chemical compositions of the thermal waters^[100]. In four types of geothermometers above mentioned, silica and gas geothermometers are sensitive to the reaction process after the solution equilibration, such as dilution. Evaporation, condensation, and the estimation of vapor-solution equilibrium errors all have a significant effect on the gas geothermometry^[101].

Pürschel, Gloaguen^[102] calculated the reservoir temperature of the Ethiopian rift geothermal system and found it to be 185 ± 20 °C, based on the cations geothermometry and the silica geothermometry. The results of Na-K and Na-K-Ca geothermometers are more reliable than those of Si-K, Mg-Mg, Na-K-Ca-Mg and Na-Li geothermometers in this high temperature system. Because the former two are less affected by the shallow groundwater mixing, and the rebalancing effect in the ascending process is small.

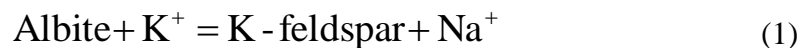
In this study, we opted to use cation geothermometers and silica geothermometers to estimate exchange temperature of the deep geothermal system in the western area of Guangdong province, and discuss the applicability of various geothermometers in combination with the existing data.

4.3.1 Cation geothermometers

The cationic geothermometers generally include Na-K geothermometer, Na-K-Ca geothermometer, K-Mg geothermometer, Na-Li geothermometer and so on^[103]. They are based on the dissolution or dissolution ratio of Na^+ , K^+ , Mg^{2+} , Ca^{2+} and Li^+ . The established equation with a certain temperature dependence is based on the cation exchange reaction. All temperature calculated by cation geothermometers are empirical approximations^[104]. In the current research study, three kinds of cation geothermometer were selected to calculate the exchange temperature, the results are shown in Table 4.

4.3.1.1 Na-K geothermometer

Orville^[105] and Hemley^[106] suggested that the sodium and potassium contents in most natural waters are controlled by the dissolution of albite and potassium feldspar in the water at higher temperatures. The existence of cation exchange between coexisting alkaline feldspars is shown in the following equation:



this formula is generally applicable to high temperature geothermal systems with long residence times and temperature above 150 °C. When the temperature is 180 ~ 200 °C, the calculated result is ideal. At this time, the albite and potassium feldspar in the water reach the equilibrium state. When the temperature of the hot water is low, the calculated results may show large deviations^[107]. Na-K geothermometer is expressed by the following equation:

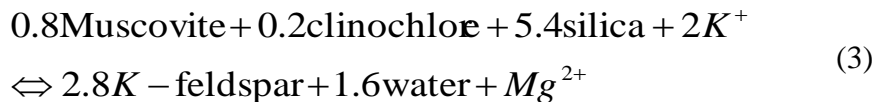
$$T_{Na-K} = \frac{933}{0.993 + \lg(C_{Na}/C_K)} - 273.15 \quad (2)$$

Where C_{Na} , C_K , respectively represent water's sodium and potassium ions concentration, mg/L.

According to the discussion of Giggenbach^[52], Na-K geothermometer indicates inaccurate results in acidic or SO_4^{2-} -concentrated solutions; but apply to near-neutral, low- SO_4^{2-} or high- CO_2 hot water. The formula is not applicable when the calcium content in the hot water is high, or the hot water is mixed with the shallow cold water^[108]. The measured temperature of hot water in this area is up to 92.7 °C, and the heat exchange temperature calculated according to the empirical formula is 134.5 ~ 662.3 °C, which is different from the measured temperature. The hot water temperature is not high, and the hot spring Ca^{2+} and SO_4^{2-} content are high, the calculated value is significantly higher than the measured value, so the formula is not applicable.

4.3.1.2K-Mg geothermometer

The K-Mg geothermometer applies to the situations where dissolved Na and Ca have not equilibrated between fluid and rock. This geothermometer re-equilibrates quickly at cooler temperatures according to the reaction:



When the deep hot water rises to the surface and mixes with the shallow cold water, the original mineral - fluid balance is disturbed by reacting with the mineral in the surrounding rock at the lower temperature and rebalances^[109]. Because of the high degree of rebalancing of potassium and magnesium minerals, the temperature calculated by this empirical formula is generally lower than the actual temperature of the deep reservoir and represents the temperature at a certain point in the ascending process^[110]. The K-Mg geothermometer responds more quickly to temperature changes and is more easily balanced in low-temperature waters, and therefore can find use in estimating shallow water temperature^[52].

K-Mg geothermometer equation:

$$T_{K-Mg} = \frac{4410}{14.0 - \lg(C_K^2 / C_{Mg})} - 273.15 \quad (4)$$

The exchange temperature calculated by this formula is 41.7 ~ 167.6 °C, which is close to the measured value, indicating that if the deep hot water mixes with the shallow cold water, the magnesium in the mixed water attains re-equilibrium. From the deep to shallow levels the hot water ascension flow rate is very fast, which makes temperature loss smaller.

4.3.1.3Na-K-Ca geothermometer

Fournier and Potter^[104] and Fournier and Truesdell^[111] proposed a formula that can be used to calculate the exchange temperature in geothermal systems with high calcium content, where the empirical coefficient β is determined from the calculated results. When the calculated temperature is less than 100 °C, empirical coefficient β takes 4/3; when the calculated temperature is greater than 100 °C, the empirical coefficient β take 1/3. d'Amore, Fancelli^[112] established according to Mg^{2+} the modified reservoir temperature formula that is suitable for medium-low temperature geothermal water^[113]

Na-K-Ca geothermometer:

$$1T_{Na-K-Ca} = \frac{1647}{2.24 + \lg(C_{Na}/C_K) + \beta \lg(C_{\sqrt{Ca}}/C_{Na})} - 273.15 \quad (5)$$

Modified Na-K-Ca geothermometer:

$$2T_{Na-K-Ca} = \frac{1647}{2.47 + \lg(C_{Na}/C_K) + \beta(\lg(C_{\sqrt{Ca}}/C_{Na}) + 2.06)} - 273.15 \quad (6)$$

In the equation (5), when β takes 4/3, the calculated result is negative or greater than 100 °C, the result is contrary to the use of the formula. When β takes 1/3, the calculated results are much higher than the measured temperature, and not applicable.

Using equation (6) (modified), the exchange temperature estimation at sampling points 1, 2, 15, 16 and 19 taking $\beta = 1/3$ is reasonable. Then, the calculated temperature of the remaining hot water sampling point is deduced by combining the geologic background of the unknown temperature sampling point and the position of the sampling point of the determined temperature. Finally, the exchange temperature of all hot water sampling points is calculated. The calculated exchange temperature range was 135.2 °C ~ 263.5 °C and the average value was 171.9 °C.

Table 4. Temperature of geothermal reservoirs calculated by various cation geothermometers.

Sample	Measured temperature (°C)	T _{Na-K}	T _{K-Mg}	1T _{Na-K-Ca} (β=4/3)	1T _{Na-K-Ca} (β=1/3)	2T _{Na-K-Ca} (β=4/3)	2T _{Na-K-Ca} (β=1/3)
1	92.7	281.5	136.2	-9493.2	492.1	315.5	263.5
2	72	197.6	82.1	1527.2	348.2	150.1	188.6
3	42	134.5	50.9	612.7	255.3	67.4	135.2
4	63.7	156.8	64.7	622.9	271.8	68.9	145.0
15	54.5	158.5	46.3	959.0	296.7	108.7	159.5
16	55.4	162.2	45.5	939.3	298.3	106.8	160.4
17	25.3	662.3	52.6	321.1	420.0	13.4	227.0
18	63.2	147.8	41.7	797.1	279.1	91.6	149.3
19	79.2	216.2	151.6	1199.4	349.5	129.0	189.3
20	77.5	171.8	55.7	840.6	299.2	96.5	160.9
21	53.5	155.4	167.6	872.0	289.4	99.9	155.3
22	45	146.9	43.5	738.1	274.3	84.5	146.5
23	42.2	160.2	46.3	788.6	287.5	90.6	154.2
average	58.9	211.7	75.7	851.5	320.1	109.5	171.9

4.3.2 Silica geothermometers

Quartz, chalcedony, tridymite, cristobalite, coesite, stishovite and amorphous silica are different stable phases of naturally found silica. The dissolution-precipitation equilibration of such multi-phase minerals depends upon the solution-host rock contact time, and its definition requires an understanding of mineral-solubility kinetics^[1]. Commonly used silica geothermometers are quartz and chalcedony geothermometers, they are based on the relationship between solubility of hot water SiO₂ and temperature^[8].

Because of the difference in solubility of SiO₂ minerals in hot water, their dissolution equilibrium temperature is different. Therefore, when this geothermometer is applied to estimate the exchange temperature, it is necessary to identify which minerals

control the solubility of SiO₂ in the hot water. Kennedy ^[115] suggested that the solubility of salt in water and the density of the solution have a very big connection. It is considered that the dissolved silica reaches a maximum value (about 330 °C) along the vapor pressure curve at a high temperature. The density of the solution decreases rapidly as the temperature further increases, meanwhile the dissolved silica content also decreases^[116]. When the temperature is less than 340°C, the solubility of SiO₂ in hot water increases with increasing temperature. In general, quartz geothermometer is suitable in high exchange temperature (> 120 to 180°C) chalcedony geothermometer applies to low temperature geothermal conditions (<110 °C)[102]

Pasvanoğlu and Chandrasekharam ^[117] estimated the exchange temperature in the Nevsehir region of central Turkey through different silica geothermometers. They noticed that there is difference in the calculated results, which means that silica in the mineralized water was precipitated as the solution rose, indicating that the silica geothermometer in the region was not applicable.

Fournier and Rowe ^[116] suggested that when calculating the underground exchange temperature of the hot spring water from the deep high pressure area to the surface atmospheric pressure area using the silica geothermometer, the amount of steam separated from the water should be corrected.

One of the estimation methods is to assume that there is adiabatic cooling, the entropy or enthalpy of the same value and this method must meet two conditions in the application: (1) cooling method for the steam loss, (2) calculated temperature value is the last quartz equilibrium temperature. When the quartz precipitates as the hot water rises to the surface and cools, this method estimates a low temperature. This may happen to hot water containing many gases such as CO₂, H₂S, etc., which leave the solution as it ascends and take away the heat from the system, thereby reducing the amount of steam formed. The mixing of hot water with relatively dilute or shallow cold water results in a lower temperature estimation.

Cooling of the hot water in the host-rock affects the dissolution equilibrium temperature of the mineral. Conductive or adiabatic cooling leads to polymerization or precipitation of the silica in the solution, resulting in a low calculated reservoir temperature^[118]. Fournier ^[101] Fournier and Rowe ^[116] established a quartz-based hot water conductive cooling and maximum steam loss in the case of adiabatic cooling of the two geothermal temperature scale.

Quartz geothermometer (conduction cooling):

$$T1 = \frac{1309}{5.19 - \lg S} - 273.15 \quad (7)$$

Quartz geothermometer (maximum steam loss):

$$T2 = \frac{1522}{5.75 - \lg S} - 273.15 \quad (8)$$

At the same time, Fournier ^[101] proposed a temperature-based formula for the dissolution equilibrium of chalcedony in hydrothermal solutions. Subsequently, ^[107]based on the results of field investigation established an equation for reservoir temperature estimation.

Chalcedony geothermometer:

$$T3 = \frac{1000}{4.78 - \lg S} - 273.15 \quad (9)$$

$$T4 = \frac{1112}{4.91 - \lg S} - 273.15 \tag{10}$$

Verma and Santoyo ^[119] developed a modified formula to estimate temperature by silica geothermometer ($SiO_2 < 295 \text{ mg/L}$).

$$T5 = -44.119 + 0.244695 - 1.7424 \times 10^{-4} + 79.305 \lg S \tag{11}$$

Where S is the dissolved SiO_2 content of the solution.

As the hot water rises, the pressure decreases, the solubility of silica will be reduced, so hot water SiO_2 content reaches its saturation easily. When the calculated results of SiO_2 geothermometer are close to the measured temperature, the ascending flow rate of the underground hot water is very high. Exchange temperature calculated according to the empirical formula of SiO_2 geothermometer are shown in Table 5, most of the calculated values are lower than the measured value, the results are too small. From the measured dissolved SiO_2 content it can be seen, in addition to individual sampling points that silica in hot water undergoes little changes. This indicates that SiO_2 is precipitated during the process of hot water rising from deep reservoir to the surface, so the estimation result of SiO_2 geothermometer is not applicable. Mixing with shallow water has little effect on Na / K ratio in geothermal waters, but it has a great effect on the dissolution of SiO_2 . As a result of the mixing effect of shallow cold water, the calculated results based on SiO_2 geothermometer are far less than the actual exchange temperature^[2].

Table 5. Temperature of geothermal reservoirs calculated by silica geothermometers.

Sample	Measured temperature (°C)	Dissolved SiO_2 (mg/L)	$\lg(SiO_2)$	T1	T2	T3	T4	T5
1	92.7	51.62	1.71	103.3	103.8	52.9	74.7	104.3
2	72	4.77	0.68	17.0	27.0	-29.3	-10.3	10.9
3	42	13.44	1.13	49.1	56.2	0.7	20.9	48.7
4	63.7	17.14	1.23	57.7	63.9	8.9	29.4	57.9
15	54.5	15.88	1.20	55.0	61.4	6.2	26.6	55.0
16	55.4	17.73	1.25	59.0	65.0	10.0	30.6	59.2
17	25.3	4.87	0.69	17.6	27.5	-28.8	-9.8	11.6
18	63.2	13.49	1.13	49.3	56.3	0.8	21.0	48.8
19	79.2	18.12	1.26	59.8	65.7	10.8	31.3	60.1
20	77.5	22.79	1.36	68.4	73.4	19.1	39.9	69.1
21	53.5	11.88	1.07	44.9	52.4	-3.2	16.8	44.0
22	45	19.68	1.29	62.8	68.4	13.7	34.4	63.3
23	42.2	22.31	1.35	67.6	72.6	18.3	39.1	68.3

4.4 Water-rock interaction in geothermal system

It can be seen from geothermometry results that the calculated temperatures of different geothermometers have great difference for the same sampling point. This is

because each geothermometry is a kind of empirical formula and has a certain application conditions. Therefore, we must determine the reservoir temperature on basis of the mineral-fluid balance in combination with the actual conditions and selecting the appropriate geothermometry.

This technique for the derivation of Na-K-Mg-Ca geoinicators was proposed by Giggenbach [52] as one of the classification techniques for different kinds of water depending on whether they are: 1) immature water; 2) partially equilibrated water; or 3) fully equilibrated water. Using the plots, one may apply geothermometers to the equilibrated and partially equilibrated water only. The triangular diagram, which is temperature dependent, is based on two reactions:

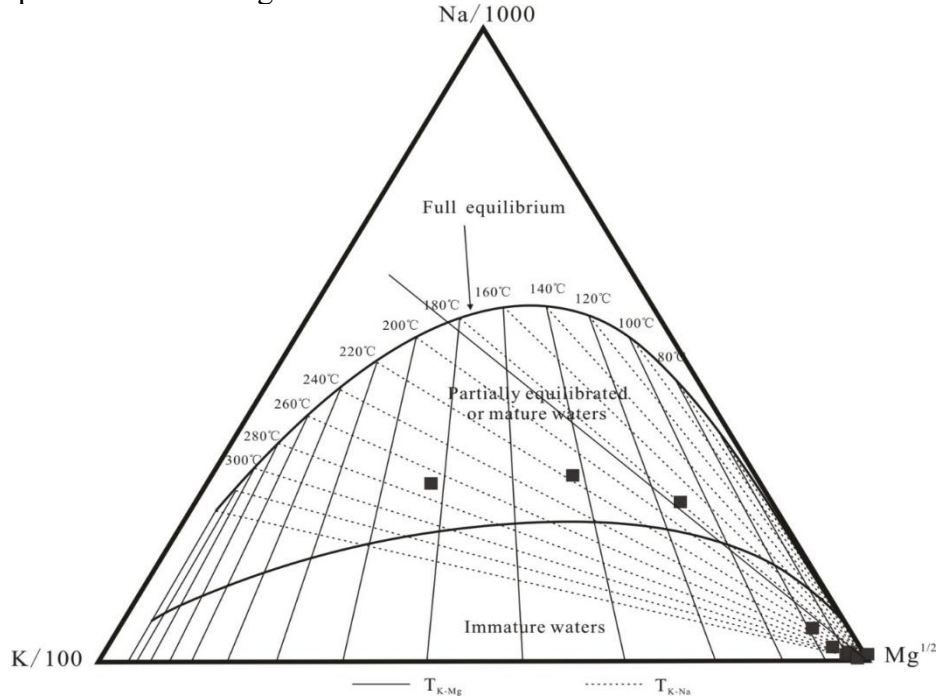
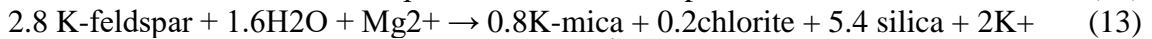
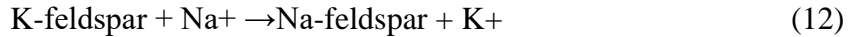


Fig. 8 The Na-K-Mg triangular diagram for the hot waters

The formula for calculating the coordinate of the water sample in the Na-K-Mg triangular diagram is:

$$S = C_{Na}/1000 + C_K/100 + \sqrt{C_{Mg}} \quad (14)$$

$$Na\% = C_{Na} / 10S \quad (15)$$

$$K\% = C_K / S \quad (16)$$

$$Mg\% = 100\sqrt{C_{Mg}} / S \quad (17)$$

Where CNa, CK, CMg were sodium, potassium, magnesium ion concentration, in mg/L.

The contents of Na⁺, K⁺ and Mg⁺ in the underground hot water collected in the study area are projected into triangles as shown in Fig. 8. From the Na-K-Mg triangular diagram, it can be seen that all the hot water sampling points in the study area are close to the Mg end element at the lower right corner, which shows the water-rock equilibrium temperature is low, and the sodium and potassium minerals in the hot water are not in a saturated state. The temperature of the hot spring water is approximately 185 °C, which

is close to that of the Na-K-Ca geothermometer. It indicates that the deep high-temperature geothermal water mixed with the shallow-cold water, the original equilibrium of hot water has been changed by dilution with cold water which forms an immature water. At the point of partial equilibrium, the share of cold water mixed is small.

The hot water spots converge at the Mg end, indicating that the hot water reached the shallow and cold water mixture, Mg in hot water to achieve a rebalance^[117] At this point, K-Mg calculated temperature is too small and does not yield the true exchange temperature. The exchange temperature calculated using the Na-K and K-Mg geothermometers in the study area is inaccurate. The calculated temperature of Na-K, and Na-K-Ca is much higher than that of K-Mg geothermometer, which indicates that Na-K-Ca geothermometer is less affected by mixing. Saturation index expresses the characteristic value of the degree of saturation of a mineral in groundwater, generally expressed as SI. When $SI > 0$, it means that the dissolution of a mineral in the groundwater is already in the supersaturation state, and the mineral will precipitate from the groundwater. $SI = 0$ indicates that the groundwater is in equilibrium with the mineral; $SI < 0$ reflects the groundwater in the dissolution of the mineral has not yet reached saturation, it can dissolve more of the mineral^[120]

In this research, PHREEQCI is used to calculate the mineral saturation index of hot spring. This software is widely used in the calculation of geochemical parameters of low temperature water-bearing system. The saturation index SI of the hot water in the study area simulated by PHREEQCI is shown in Table 6.

The dissolved SiO_2 in the solution did not reach the saturated state, and the mineral saturation index of chalcedony and quartz fluctuated in the range of -0.5 to 0.5. Among them, the chalcedony is generally in a saturated state, representing the deep geothermal fluid and shallow mixed water temperature. The saturation index of quartz is closer to 0, indicating that quartz is close to equilibrium and that the original silica content in the hot water is retained and does not reach rebalance in the cycle. This stabilization may be due to the rapid flow of hot water in the deep faults and to the fact that there is almost no loss of heat when passing through the cold bedrock. The quartz geothermometer is generally used in high temperature geothermal system for temperature estimation. It is not applicable in the study area.

Albite, gypsum, celestite and other with $SI < -0.5$, are in the unsaturated state; chlorite, dolomite, mica and other minerals with $SI > 0.5$, are in a state of supersaturation. Feldspar minerals, sulphate minerals and aluminosilicate minerals are not saturated, indicating that hot water mixed with a shallow water unsaturated in the mentioned minerals. The fluorite minerals in the water are saturated ($SI = 0.1$) and the main component of the fluorite is CaF_2 , so the fluorine and calcium contents in the hot water are very high, which is in a good agreement with the previous discussion.

Table 6. Saturation indices of main minerals of the water samples.

mineral	SI	mineral	SI	mineral	SI
Albite	-3.52	Celestite	-3.37	Chalcedony	-0.49
Alunite	-17.16	Illite	-3.74	Quartz	-0.11
Anglesite	-5.32	K-feldspar	-2.54	Dolomite	0.76
Anhydrite	-3.5	Barite	-1.48	Fluorite	0.1
Anorthite	-5.09	$SiO_2(a)$	-1.27	Calcite	0.01
Ca-Montmorillonite	-4.36	Kaolinite	-1.93	K-mica	0.57
Gypsum	-3.38	Gibbsite	-1.3	Sepiolite	1.09

Halite	-7.08	Aragonite	-0.12	Chlorite(14A)	7.85
--------	-------	-----------	-------	---------------	------

4.5 Geothermal water circulation depth

As the atmospheric precipitation water descends along the deep faults its temperature increases. Using empirical formulae, the circulation depth of the groundwater can be estimated. According to the existing data on geothermal characteristics of southern China, the geothermal gradient is between 7.82 and 162.5 °C / km, with an average value of 24.1 °C / km^[1]. The range of coordinates is about 111 ° 00'~ 112 ° 30' east longitude and 21 ° 20'~ 22 ° 20' north latitude. The geothermal gradient is 25 ~ 35 °C / km, and the average geothermal gradient is 30 °C / km which have been used in this thesis to calculate the circulation depth of geothermal water.

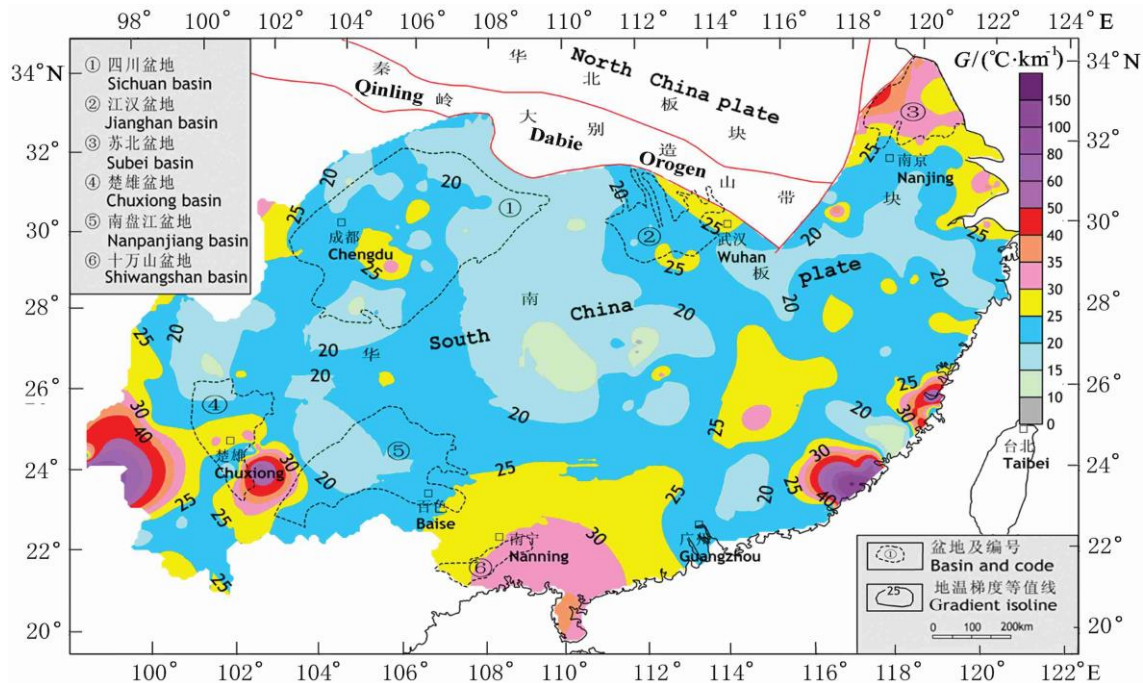


Fig. 9 The China southern continental geothermal gradient^[1]

Through the analysis of the previous geological conditions, we can see that groundwater temperature in the geothermal system is simply obtained from the internal earth heat system. The formula for estimating the circulation depth of the hot spring is ^[121]:

$$Z = G(T_z - T_0) + Z_0 \tag{18}$$

Where Z is the circulation depth of geothermal water, expressed in m; G, the geothermal gradient of the study area in m/°C; Tz, the underground heat storage temperature in °C; T₀, the annual average temperature of the recharge area in °C and Z₀ is the normal temperature zone expressed in m. Experimentally calculated G value is 33m /°C, Tz value of 42.0 ~ 92.7 °C, T₀ value of 22.5 °C, and Z₀ take 13m. The geothermal water circulation depth is estimated between 105.4m and 2329.6 m, which indicates a maximum circulation depth of the geothermal water in the study area to be 2329.6m.

4.6 ¹⁴C Age Correction

4.6.1 Correction of the traditional model

The traditional models and methods are widely used in the ¹⁴C age correction. According to the existing conditions and related data in the study area, six kinds of calibration methods are used, that is: CMB, Tamers, Pearson, Gofiantinic, Mook and Fontes-Garbier.

CMB: The ¹⁴C concentration of the shallow groundwater in the recharge area is used as the initial ¹⁴C concentration as follows:

$$t = 8267 \times \ln \frac{A_{rech}}{A_T} \quad (19)$$

Tamers: Based on the chemical equilibrium of carbonate, the initial concentration is calculated as follows:

$$A_0 = \frac{[m_{CO_2}] + [0.5m_{HCO_3^-}]}{[m_{CO_2}] + [m_{HCO_3^-}]} A_{soil} \text{ (%mod)} \quad (20)$$

Pearson: The formula for the correction based on the mass balance principle is as follows:

$$A_0 = \frac{[\delta^{13}C_{DIC}] - [\delta^{13}C_{carb}]}{[\delta^{13}C_{soil}] - [\delta^{13}C_{carb}]} (A_{soil} - A_{carb}) + A_{carb} \text{ (%mod)} \quad (21)$$

Gofiantini: An isotopic mixing-exchange model is proposed based on the isotopic mixture model. Assuming the HCO₃⁻ exchange equilibrium with soil in water, subtracting the δ13C fraction from the Pearson formula yields the following equation:

$$A_0 = \frac{[\delta^{13}C_{DIC}] - [\delta^{13}C_{carb}]}{[\delta^{13}C_{soil}] + [\delta^{13}C_{fraction}] - [\delta^{13}C_{carb}]} (A_{soil} - A_{carb}) + A_{carb} \text{ (%mod)} \quad (22)$$

Mook: Based on the exchange of inorganic carbon in groundwater with soil 13C, a chemical dilution-isotope exchange model is proposed. The formula is as follows:

$$A_0 = \frac{1}{m_{DIC_{mean}}} \left[\frac{2(\delta^{13}C \cdot m_{DIC_{mean}} - \delta^{13}C_{soil} \cdot m_{DIC_{soil}})}{\delta^{13}C_{soil} - \delta^{13}C_{carb}} + \frac{\delta^{13}C_{carb} \cdot m_{DIC_{carb}}}{2\epsilon^{13}C_{CO_2-CaCO_3}} + m_{DIC_{soil}} \right] \quad (23)$$

Fontes-Garnier: According to the ion content of the mass balance relationship, the formula is as follows:

$$A_0 = \frac{m_{DIC_{mean}} - m_{DIC_{mineral}} + m_{DIC_{CO_2-exch}}}{m_{DIC_{mean}}} \cdot A_{soil} \text{ (%mod)} \quad (24)$$

The corresponding correction results are shown in Table 7.

Table 7. ¹⁴C Ages of various correction models

Sample no.	Gon	Mook	F-G	Pea	Tam	CMB
1	2224	2057	5499	2069	7203	6222
2	2867	2740	6409	2451	9474	8104
3	4926	4632	8268	3851	13305	11994
4	4217	3637	8645	3139	11175	11060
5	6385	5081	9931	4786	16761	14697
6	5621	5365	3464	3882	11310	9805
7	8203	8199	9929	7089	15359	15393
8	2725	-	9329	2033	13278	7154

9	-	-	8744	855	12772	6797
10	2102	-	6406	1769	10463	6362
11	6509	2798	10874	4940	20155	15895
12	4973	-	14472	3443	28419	21642
13	5791	-	12671	4347	16225	11736
14	8224	7327	12090	6726	20348	13889
15	7363	5894	12072	6284	22148	19055
16	8026	7670	11055	7094	17870	14918
17	8918	8816	10186	7855	17205	15317
18	2217	1848	5324	1976	6250	4369
19	83	-	4464	1078	839	2100
20	10842	10622	14326	11391	24570	19608
21	9178	8365	13605	8780	23302	17026
22	2765	2424	6370	2221	5851	994

For the actual situation of the study area, the calibration results of various models are analyzed as follows. The Vogel method is a purely statistical method that does not take into account the chemical and isotopic exchange reactions that occur during the infiltration of groundwater, and can be used in the absence of hydrochemical and isotopic data, usually with the results of the ^{14}C assay (CMB). The average corrected age is 11552a, which is 40.75% younger than the unadjusted age. However, this is obviously not in agreement with the complex water chemistry process in the study area. Tamers is a purely positive model which can be applied to closed confined aquifer systems in arid and semi-arid areas where the soil layer is thin, voids are not developed and the soil CO_2 partial pressure is medium. The mean age is 14740a, and 24.39% of uncorrected age. The fractures in the study area are rich and the CO_2 partial pressure is high, and the Tamers model is not applicable, and the calibration results are too large.

The Pearson model also takes into account the exchange process between isotopes, with an average age of 4457 a, a difference of 77.14%. Gonfiantinie average age is 5436a, a difference of 72.12%, which not only takes into account the soil carbon dioxide and solid carbon carbonate between the two carbon sources of mixed action, but also takes into account the soil CO_2 and water HCO_3^- carbon isotope exchange. Mook average age is 5467a, taking full account of the ^{13}C isotope exchange reaction between soil CO_2 and total dissolved inorganic carbon, is more suitable for closed confined aquifer system in the tropics with thicker soil layer and higher $\delta^{13}\text{C} \pm \text{CO}_2$ value. The exchange process between HCO_3^- and solid carbonate rock in aquifer is considered. Fonters and Garnier average age is 9279a and takes into account both the dilution effect and the isotope exchange reaction. These three model corrections take into account the complexity of the study area and may be closer to the real age.

The ^{14}C ages calculated by various models are significantly smaller than the uncalibrated ages, especially considering the more complex correction model of the water chemistry process. However, there are some differences in the corrected ages of the various models, due to the different chemical reactions considered by the various models. The results of the correction are different and the accuracy is difficult to judge. However, the calibration results of the conventional model are also instructive. The calibration results are much different from the uncorrected results, indicating the need for correction of geothermal water ages.

4.6.2 Improved calibration methods

4.6.2.1 Reverse Chemical Simulation

Reverse chemical modeling is based on the mass balance reaction model and the isotopic mass transfer model. In the water flow path, the end point of the water chemistry and isotope composition is equivalent to the starting point of the corresponding components plus the process of water-rock interaction and the role of different water mixing and evaporation concentration caused by the amount of change. The expression is:

$$\sum_{p=1}^p a_p b_{p,k} = m_{T,k}(\text{final}) - m_{T,k}(\text{initial}), \quad K = 1, 2, \dots, J \quad (25)$$

P represents the number of reaction phases (possible minerals); a_p represents the amount of the pth mineral or gas entering the material leaving the groundwater; b_p, k represents the stoichiometry of the compound k in the pth mineral species; $m_{T, k}$ Represents the total molar mass concentration of the compound k; J is the number of elements included.

According to the above equation, it is necessary to carry out reverse chemical simulation of the chemical composition of the starting point and the end point of the water flow path, that is, the constraint variable and the mineral species involved in water-rock interaction. Under different mass balance equations, that is, reaction model, different water chemistry reaction results are obtained, and the most suitable model is selected as the geochemical action of groundwater path.

On this basis, the carbon isotope as a constraint variable, the establishment of the reaction path in the mass transfer model to shallow groundwater as a starting point. NO_3^- is affected by human activities and denitrification, it is difficult to establish its mass balance equation. By use of PHREEQCI software we calculated the saturation index of the seven main minerals, comprehensively selected, which are calcite, aragonite, dolomite, gypsum, anhydrite, potassium feldspar and plagioclase. The $\delta^{13}\text{C}$ of the calcite, calcite and dolomite is given as 0 ‰ and ^{14}C is 0pmc. Using the NETPATH software for the start-point correction to get the transmission age, here we suppose that the age of the recharge area is 0a, thus we can determine the corrected age. The calibration results are shown in Table 8.

Table 8. ^{14}C ages calibration results

Sample no.	^{14}C (pmc,%)	starting point	Starting point calibration	Reverse chemical simulation
1	23.84	50.74	42.45	4770
2	18.97	50.74	37.30	5590
3	11.83	50.74	28.56	7285
4	13.25	50.74	30.45	6878
5	8.52	50.74	23.72	8464
6	15.43	50.74	33.19	6332
7	7.83	50.74	22.61	8767
8	12.89	30.72	29.98	6977
9	13.46	30.72	30.72	6822
10	14.19	30.72	31.65	6632
11	4.46	30.72	16.45	10788
12	2.22	30.72	11.08	13292
13	7.39	30.72	21.88	8975

14	5.69	30.72	18.87	9913
15	3.97	40.13	15.40	11206
16	6.56	40.13	20.46	9402
17	6.25	40.13	19.90	9576
18	23.61	40.13	42.22	4804
19	45.38	58.56	61.09	2458
20	2.58	27.89	12.07	12753
21	3.53	27.89	14.41	11627
22	24.72	27.89	43.33	4639

The average value of the reverse chemical simulation is 8089a, and the good part of this result is that the water-rock interaction is considered as an important influencing factor, which is reliable. Compared with the traditional model, the corrected age values are significantly smaller than those of the CMB and Tamers models, which are larger than those of the Gon, Pea and Mook models, which are close to the F-G model.

4.6.2.2 Correction for the ¹⁴C depleted carbonates

The possibility of deep-seated CO₂, discussed earlier, is based on the Pearson model, which can be modified to take account of the dilution of CO₂ from deep sources. The results show that the δ¹³C value of deep CO₂ is -1.5 ‰, and the δ¹³C_{rech} of the recharge zone is calculated by the same principle. The formula for calculating the CO₂ dilution factor is as follows:

$$q = \frac{\delta^{13}C_{DIC} - \delta^{13}C_{carb}}{\delta^{13}C_{rech} - \delta^{13}C_{carb}} \tag{26}$$

The ¹⁴C age is thus calculated as shown in Table 9.

Table 9. Results of the Correction for the ¹⁴C depleted carbonates

Sample no.	¹⁴ C (pmc, %)	δ ¹³ C (PDB, ‰)	q	Improved model
1	23.84	-10.17	0.35	3124
2	18.97	-9.82	0.31	4110
3	11.83	-10.53	0.24	5771
4	13.25	-9.18	0.24	4847
5	8.52	-10.02	0.19	6814
6	15.43	-13.87	0.26	4222
7	7.83	-15.94	0.18	6669
8	12.89	-5.39	0.26	5786
9	13.46	-2.2	0.26	5396
10	14.19	-5.08	0.25	4530
11	4.46	-5.47	0.13	8683
12	2.22	-1.72	0.09	11197
13	7.39	-7.67	0.22	9048
14	5.69	-10.72	0.15	7814
15	3.97	-6.78	0.13	9983
16	6.56	-13.37	0.18	8117
17	6.25	-14.87	0.15	7469
18	23.61	-9.56	0.33	2713
19	45.38	-9.48	0.48	424
20	2.58	-11.48	0.09	10666
21	3.53	-10.02	0.13	10664

22
24.72
-11.43
0.34
2708

The average corrected age of the improved method is 6398a, which is consistent with that of reverse chemical simulation. However, in the process of formation of geothermal water in the study area, the origin of "dead carbon" is not negligible. Such a correction method on the data requirements are relatively high, and is likely to cause excessive correction. The actual age of the study area should be less than that of the reverse chemical simulation, and it is more reliable than the modified correction method in this section, as the "real age".

5. Concluding Remarks

Deep faults zone of western Guangdong are mainly found in granite clastic rock fissures and host geothermal waters of meteoric origin as confirmed by oxygen and hydrogen isotopes characteristics. The geothermal waters of this area are geochemically carbonic acid water type to chlorine water from inland to coastal areas. Calculated temperatures for the same water samples using different geothermometers shown discrepancies. Considering the mineral saturation indices calculated by PHREEQCI software, mineral saturation by Na-K-Mg triangular diagram we can see that the optimum geothermometer is the Na-K-Ca geothermometer which estimates the reservoir temperature value between 135.2-263.5°C and 171.9°C on average.

The estimated temperature is high and may support the dissolution of “dead carbon” carbonates from the host rock to the geothermal waters, hence a necessity of recalibration when estimating the residence of the geothermal waters in the underground. The residence time calculated in Guangdong geothermal waters ranges between 1141- 12245a, an average of 7243a. From the deep geothermal reservoir, ascending hot water mixes with cold groundwater of the shallow levels. After mixing, the temperature is not high and potassium and sodium minerals are out of balance.

Our work is not that perfect. We would like to make more consistent work, but it has been not easy for us due to time constraints. That is why we propose the following recommendations for future research:

1. For a better and improved interpretation of chemical and isotopic characteristics, the number of sample used in the study should be increased. It is relatively uncertain to rely on few samples distributed in large study area.
2. For purposes of comparison and consistency of the research, some gaseous components such as CH₄, CO₂ and some isotopes such as ³He/⁴He, ³²S/³⁴S, etc. should be included in the future studies.
3. In this research some parameters have determined based on empirical formulae, this include the circulation depth, hot and cold water mixing ratio etc. We suggest that in the future these parameters should be based on the field measurement.

References

1. Yuan, Y., Y. Ma, and S. Hu, Characteristics of geothermal geology in southern China Chinese Journal of Geophysics, 2006. 04: p. 1118-1126.
2. Nicholson, K., Geothermal fluids: chemistry and exploration techniques. 2012: Springer Science & Business Media.
3. Williams, C.F., M.J. Reed, and A.F. Anderson. Updating the classification of geothermal resources. in Proceedings, Thirty-Sixth Workshop on Geothermal Reservoir Engineering. 2011.
4. van Leeuwen, W.A., Geothermal exploration using the magnetotelluric method, 2016, UU Dept. of Earth Sciences.
5. Edenhofer, O., et al., Renewable energy sources and climate change mitigation: Special report of the intergovernmental panel on climate change. 2011: Cambridge University Press.
6. Lu, G., et al., Deep geothermal processes acting on faults and solid tides in coastal Xinzhou geothermal field, Guangdong, China. Physics of the Earth and Planetary Interiors, 2016.

7. Spycher, N., et al., Integrated multicomponent solute geothermometry. *Geothermics*, 2014. 51: p. 113-123.
8. Arnórsson, S., The use of mixing models and chemical geothermometers for estimating underground temperatures in geothermal systems. *Journal of Volcanology and Geothermal Research*, 1985. 23(3): p. 299-335.
9. Spera, F.J. and W.A. Bohron, Energy-constrained open-system magmatic processes I: General model and energy-constrained assimilation and fractional crystallization (EC-AFC) formulation. *Journal of Petrology*, 2001. 42(5): p. 999-1018.
10. Guo, R., H. Gui, and L.C. Guo, *Interprovincial Cooperation and Development, in Multiregional Economic Development in China*. 2015, Springer. p. 173-460.
11. Ueda, A., et al., Experimental studies of CO₂-rock interaction at elevated temperatures under hydrothermal conditions. *Geochemical Journal*, 2005. 39(5): p. 417-425.
12. Lu, Z.-T., et al., Tracer applications of noble gas radionuclides in the geosciences. *Earth-science reviews*, 2014. 138: p. 196-214.
13. Zhou, Y., et al., Hydrothermal origin of Late Proterozoic bedded chert at Gusui, Guangdong, China: petrological and geochemical evidence. *Sedimentology*, 1994. 41(3): p. 605-619.
14. LIU, Z.-z., et al., Evaluation of Agricultural Suitability on Geothermal Water in Guangdong [J]. *Journal of Natural Resources*, 2011. 1: p. 013.
15. Wang, P., Q. Li, and C.-F. Li, *Geology of the China Seas*. Vol. 6. 2014: Elsevier.
16. Sun, Z., et al. Radiogenic heat production of granites and potential for hot dry rock geothermal resource in Guangdong Province, Southern China. in *Proceedings world geothermal congress*. 2015.
17. Zhou, b.X., et al., Petrogenesis of Mesozoic granitoids and volcanic rocks in South China: a response to tectonic evolution. *Episodes*, 2006. 29(1): p. 26.
18. Li, X.-H., et al., Jurassic intraplate magmatism in southern Hunan-eastern Guangxi: ⁴⁰Ar/³⁹Ar dating, geochemistry, Sr-Nd isotopes and implications for the tectonic evolution of SE China. *Geological Society, London, Special Publications*, 2004. 226(1): p. 193-215.
19. Mao, J., et al., Spatial-temporal distribution of Mesozoic ore deposits in South China and their metallogenic settings. *Geological Journal of China Universities*, 2008. 14(4): p. 510-526.
20. Wang, Y., et al., Phanerozoic tectonics of the South China Block: key observations and controversies. *Gondwana Research*, 2013. 23(4): p. 1273-1305.
21. Cinti, D., et al., Geochemistry of thermal waters along fault segments in the Beas and Parvati valleys (north-west Himalaya, Himachal Pradesh) and in the Sohna town (Haryana), India. *Geochemical Journal*, 2009. 43(2): p. 65-76.
22. Zhao, B., et al., Shear velocity and V_p/V_s ratio structure of the crust beneath the southern margin of South China continent. *Journal of Asian Earth Sciences*, 2013. 62: p. 167-179.
23. Sibson, R., Fault rocks and fault mechanisms. *Journal of the Geological Society*, 1977. 133(3): p. 191-213.
24. Curewitz, D. and J.A. Karson, Structural settings of hydrothermal outflow: Fracture permeability maintained by fault propagation and interaction. *Journal of Volcanology and Geothermal Research*, 1997. 79(3): p. 149-168.
25. Henley, R.W. and A.J. Ellis, Geothermal systems ancient and modern: a geochemical review. *Earth-science reviews*, 1983. 19(1): p. 1-50.
26. Dickson, M.H. and M. Fanelli, *Geothermal energy: utilization and technology*. 2013: Routledge.
27. D'Amore, F. and C. Panichi, Evaluation of deep temperatures of hydrothermal systems by a new gas geothermometer. *Geochimica et Cosmochimica Acta*, 1980. 44(3): p. 549-556.
28. Stumm, W. and J.J. Morgan, *Aquatic chemistry: chemical equilibria and rates in natural waters*. Vol. 126. 2012: John Wiley & Sons.
29. Martin, J., Analysis of internal steam drive in geothermal reservoirs. *Journal of Petroleum Technology*, 1975. 27(12): p. 1,493-1,499.
30. Segall, P. and S.D. Fitzgerald, A note on induced stress changes in hydrocarbon and geothermal reservoirs. *Tectonophysics*, 1998. 289(1): p. 117-128.

31. Moore, J.N., D.I. Norman, and B.M. Kennedy, Fluid inclusion gas compositions from an active magmatic–hydrothermal system: a case study of The Geysers geothermal field, USA. *Chemical Geology*, 2001. 173(1): p. 3-30.
32. Duchi, V., A. Minissale, and R. Rossi, Chemistry of thermal springs in the Larderello-Travale geothermal region, southern Tuscany, Italy. *Applied geochemistry*, 1986. 1(6): p. 659-667.
33. Ozgener, L., A. Hepbasli, and I. Dincer, Energy and exergy analysis of geothermal district heating systems: an application. *Building and Environment*, 2005. 40(10): p. 1309-1322.
34. Gupta, H.K. and S. Roy, *Geothermal energy: an alternative resource for the 21st century*. 2006: Elsevier.
35. Kimura, J.-I., et al., Isotope geochemistry of early Kilauea magmas from the submarine Hilina bench: the nature of the Hilina mantle component. *Journal of Volcanology and Geothermal Research*, 2006. 151(1): p. 51-72.
36. Kaszuba, J.P., D.R. Janecky, and M.G. Snow, Experimental evaluation of mixed fluid reactions between supercritical carbon dioxide and NaCl brine: Relevance to the integrity of a geologic carbon repository. *Chemical Geology*, 2005. 217(3): p. 277-293.
37. Payne, B.R., The status of isotope hydrology today. *Journal of Hydrology*, 1988. 100(1-3): p. 207-237.
38. Stănăşel, O. and L. Gilău. Interpretation of geochemical data from wells in the western geothermal field of Romania. in *Proceedings of the International Geothermal Conference, Reykjavík*. 2003.
39. Mao, X., et al., Geochemical and isotopic characteristics of geothermal springs hosted by deep-seated faults in Dongguan Basin, Southern China. *Journal of Geochemical Exploration*, 2015. 158: p. 112-121.
40. Hochstein, M., *Classification and assessment of geothermal resources. Small geothermal resources: A guide to development and utilization*, UNITAR, New York, 1990: p. 31-57.
41. Warren, J., Dolomite: occurrence, evolution and economically important associations. *Earth-Science Reviews*, 2000. 52(1): p. 1-81.
42. Ford, D. and P.D. Williams, *Karst hydrogeology and geomorphology*. 2013: John Wiley & Sons.
43. Craig, H., Isotopic variations in meteoric waters. *Science*, 1961. 133(3465): p. 1702-1703.
44. Craig, H., The isotopic geochemistry of water and carbon in geothermal areas. *Nuclear Geology on Geothermal Areas*, 1963: p. 17-53.
45. Ellis, A. and W. Mahon, Natural hydrothermal systems and experimental hot water/rock interactions (Part II). *Geochimica et Cosmochimica Acta*, 1967. 31(4): p. 519-538.
46. Frape, S. and P. Fritz, The chemistry and isotopic composition of saline groundwaters from the Sudbury Basin, Ontario. *Canadian Journal of Earth Sciences*, 1982. 19(4): p. 645-661.
47. Barbier, E., Geothermal energy technology and current status: an overview. *Renewable and Sustainable Energy Reviews*, 2002. 6(1): p. 3-65.
48. Yardley, B.W., The role of water in the evolution of the continental crust. *Journal of the Geological Society*, 2009. 166(4): p. 585-600.
49. Connolly, J.A., The mechanics of metamorphic fluid expulsion. *Elements*, 2010. 6(3): p. 165-172.
50. Markl, G., F. Von Blanckenburg, and T. Wagner, Iron isotope fractionation during hydrothermal ore deposition and alteration. *Geochimica et Cosmochimica Acta*, 2006. 70(12): p. 3011-3030.
51. Ague, J.J., Extreme channelization of fluid and the problem of element mobility during Barrovian metamorphism. *American Mineralogist*, 2011. 96(2-3): p. 333-352.
52. Giggenbach, W.F., Geothermal solute equilibria. derivation of Na-K-Mg-Ca geothermometers. *Geochimica et cosmochimica acta*, 1988. 52(12): p. 2749-2765.
53. Benderitter, Y. and G. Cormy, Possible approach to geothermal research and relative costs. *Small geothermal resources: A guide to development and utilization*, UNITAR, New York, 1990: p. 59-69.

54. Pauwels, H., C. Fouillac, and A.-M. Fouillac, Chemistry and isotopes of deep geothermal saline fluids in the Upper Rhine Graben: Origin of compounds and water-rock interactions. *Geochimica et Cosmochimica Acta*, 1993. 57(12): p. 2737-2749.
55. Chiodini, G., et al., Fluid geochemistry of Nisyros island, Dodecanese, Greece. *Journal of volcanology and geothermal research*, 1993. 56(1-2): p. 95-112.
56. Rowe Jr, G.L., Oxygen, hydrogen, and sulfur isotope systematics of the crater lake system of Poas Volcano, Costa Rica. *Geochemical Journal*, 1994. 28(3): p. 263-287.
57. Lowenstern, J.B., et al., Origins of geothermal gases at Yellowstone. *Journal of Volcanology and Geothermal Research*, 2015. 302: p. 87-101.
58. Rinehart, J.S., *Geysers and geothermal energy*. Vol. 223. 1980: Springer.
59. Hedenquist, J.W. and R.W. Henley, Hydrothermal eruptions in the Waiotapu geothermal system, New Zealand; their origin, associated breccias, and relation to precious metal mineralization. *Economic geology*, 1985. 80(6): p. 1640-1668.
60. Cook, P.G. and J.-K. Böhlke, Determining timescales for groundwater flow and solute transport, in *Environmental tracers in subsurface hydrology*. 2000, Springer. p. 1-30.
61. Magee, J.W., et al., Evaluating Quaternary dating methods: Radiocarbon, U-series, luminescence, and amino acid racemization dates of a late Pleistocene emu egg. *Quaternary Geochronology*, 2009. 4(2): p. 84-92.
62. Vogel, J.C., Investigation of groundwater flow with radio carbon., in *Isotopes in Hydrology 1967*, IAEA: Vienna. p. 225 ~ 239.
63. Han, L. and L. Plummer, A review of single-sample-based models and other approaches for radiocarbon dating of dissolved inorganic carbon in groundwater. *Earth-Science Reviews*, 2016. 152: p. 119-142.
64. Gonfiantini, R. Carbon isotope exchange in karst groundwater. in *21st Congress on Karst Hydrology and Karst Environment Protection*. 1988.
65. Vogel, J., Carbon-14 dating of groundwater, *Isotope Hydrology 1970*, 225-239, Int. At. Energy Agency, Vienna, Austria, 1970.
66. Tamers, M., Radiocarbon ages of groundwater in an arid zone unconfined aquifer. *Isotope techniques in the hydrologic cycle*, 1967: p. 143-152.
67. Pearson, F. and D. White, Carbon 14 ages and flow rates of water in Carrizo Sand, Atascosa County, Texas. *Water Resources Research*, 1967. 3(1): p. 251-261.
68. Mook, W., The dissolution-exchange model for dating groundwater with ^{14}C , in *Interpretation of environmental isotope and hydrochemical data in groundwater hydrology*. 1976.
69. Mook, W., On the reconstruction of the initial ^{14}C content of ground water from the chemical and isotopic composition, paper presented at 8th International Radiocarbon Conference, R. Soc. of New Zealand, Wellington, 1972.
70. Fontes, J.C. and J.M. Garnier, Determination of the initial ^{14}C activity of the total dissolved carbon: A review of the existing models and a new approach. *Water resources research*, 1979. 15(2): p. 399-413.
71. Tamers, M., Validity of radiocarbon dates on ground water. *Geophysical surveys*, 1975. 2(2): p. 217-239.
72. Lin, W.-j., et al., The assessment of geothermal resources potential of China. *Geol China*, 2013. 40: p. 312-321.
73. Zhang, X., X. Liang, and J. Sun, Hydrochemical characteristic and modeling of the mixture action in Qicun geothermal field. *Hydrogeology and Engineering Geology*, 2007. 6: p. 95-99.
74. Chang, J., et al., A review on the energy production, consumption, and prospect of renewable energy in China. *Renewable and Sustainable Energy Reviews*, 2003. 7(5): p. 453-468.
75. Ascough, P., et al., An Icelandic freshwater radiocarbon reservoir effect: implications for lacustrine ^{14}C chronologies. *The Holocene*, 2011. 21(7): p. 1073-1080.

76. Zigah, P.K., Sources, biogeochemical cycling, and fate of organic matter in Lake Superior: An investigation using natural abundance radiocarbon and stable isotopes, 2012, UNIVERSITY OF MINNESOTA.
77. Landis, G. and A. Hofstra, Fluid inclusion gas chemistry as a potential minerals exploration tool: case studies from Creede, CO, Jerritt Canyon, NV, Coeur d'Alene district, ID and MT, southern Alaska mesothermal veins, and mid-continent MVT's. *Journal of Geochemical Exploration*, 1991. 42(1): p. 25-59.
78. Karingithi, C.W., S. Anorsson, and K. Gronvold, Chemical geothermometers for geothermal exploration. Short Course IV on Exploration for Geothermal Resources: United Nations University, Geothermal Training Program, Lake Vaivasha, Kenya, 2009: p. 1-22.
79. Ryan, G.A. and E. Shalev, Seismic velocity/temperature correlations and a possible new geothermometer: Insights from exploration of a high-temperature geothermal system on Montserrat, West Indies. *Energies*, 2014. 7(10): p. 6689-6720.
80. Zaher, M.A., et al., Exploration and assessment of the geothermal resources in the Hammam Faraun hot spring, Sinai Peninsula, Egypt. *Journal of Asian Earth Sciences*, 2012. 45: p. 256-267.
81. Trabelsi, S., et al., Hydrochemistry of thermal waters in Northeast Tunisia: water-rock interactions and hydrologic mixing. *Arabian Journal of Geosciences*, 2015. 8(3): p. 1743-1754.
82. Tiejun, L., OVERPRESSURE AND ITS GENERATION IN SOUTH EDGE OF THE JUNGGAR BASIN [J]. *Chinese Journal of Geology*, 2004. 2: p. 009.
83. Onyango, M.S., et al., Adsorption equilibrium modeling and solution chemistry dependence of fluoride removal from water by trivalent-cation-exchanged zeolite F-9. *Journal of Colloid and Interface Science*, 2004. 279(2): p. 341-350.
84. Montety, V.d., et al., Identifying the origin of groundwater and flow processes in complex landslides affecting black marls: insights from a hydrochemical survey. *Earth Surface Processes and Landforms*, 2007. 32(1): p. 32-48.
85. Rozanski, K., L. Araguás-Araguás, and R. Gonfiantini, Isotopic patterns in modern global precipitation. *Climate change in continental isotopic records*, 1993: p. 1-36.
86. Barnes, J.D., et al., Stable isotope ($\delta^{18}\text{O}$, δD , $\delta^{37}\text{Cl}$) evidence for multiple fluid histories in mid-Atlantic abyssal peridotites (ODP Leg 209). *Lithos*, 2009. 110(1): p. 83-94.
87. Fontes, J.C., M. Yousfi, and G. Allison, Estimation of long-term, diffuse groundwater discharge in the northern Sahara using stable isotope profiles in soil water. *Journal of Hydrology*, 1986. 86(3-4): p. 315-327.
88. Davis, S.N., D.O. Whittemore, and J. Fabryka-Martin, Uses of chloride/bromide ratios in studies of potable water. *Ground Water*, 1998. 36(2): p. 338-350.
89. Alcalá, F.J. and E. Custodio, Using the Cl/Br ratio as a tracer to identify the origin of salinity in aquifers in Spain and Portugal. *Journal of Hydrology*, 2008. 359(1): p. 189-207.
90. McCarthy, J.F., et al., Field tracer tests on the mobility of natural organic matter in a sandy aquifer. *Water Resources Research*, 1996. 32(5): p. 1223-1238.
91. White, D.E., Saline waters of sedimentary rocks. 1965.
92. Cartwright, I., T.R. Weaver, and L.K. Fifield, Cl/Br ratios and environmental isotopes as indicators of recharge variability and groundwater flow: an example from the southeast Murray Basin, Australia. *Chemical geology*, 2006. 231(1): p. 38-56.
93. Herczeg, A., S. Dogramaci, and F. Leaney, Origin of dissolved salts in a large, semi-arid groundwater system: Murray Basin, Australia. *Marine and Freshwater Research*, 2001. 52(1): p. 41-52.
94. Xu, Y., Hydrological geochemistry and stable isotope of groundwater in Cangzhou City, in China University of Geosciences (Beijing)2009.
95. Clark, I.D. and P. Fritz, *Environmental isotopes in hydrogeology*. 1997: CRC press.
96. Burnett, W., et al., Quantifying submarine groundwater discharge in the coastal zone via multiple methods. *Science of the total Environment*, 2006. 367(2): p. 498-543.

97. Wen, X.F., et al., Water vapor and precipitation isotope ratios in Beijing, China. *Journal of Geophysical Research: Atmospheres*, 2010. 115(D1).
98. Ármannsson, H. and T. Fridriksson, Application of geochemical methods in geothermal exploration. *Short Course on Surface Exploration for Geothermal Resources*, 2009.
99. Gunderson, R., et al. Analysis of smectite clays in geothermal drill cuttings by the methylene blue method: for well site geothermometry and resistivity sounding correlation. in *Proceedings World Geothermal Congress*. 2000.
100. Rui, C., Selection of geothermometers and estimate of the temperature of geothermal reservoir in Pingdingshan 8th mine [J]. *Coal Geology & Exploration*, 2010. 1: p. 017.
101. Fournier, R., Chemical geothermometers and mixing models for geothermal systems. *Geothermics*, 1977. 5(1-4): p. 41-50.
102. Pürschel, M., R. Gloaguen, and S. Stadler, Geothermal activities in the main Ethiopian rift: hydrogeochemical characterization of geothermal waters and geothermometry applications (Dofan-Fantale, Gergede-Sodere, Aluto-Langano). *Geothermics*, 2013. 47: p. 1-12.
103. Verma, S.P., K. Pandarinath, and E. Santoyo, SolGeo: A new computer program for solute geothermometers and its application to Mexican geothermal fields. *Geothermics*, 2008. 37(6): p. 597-621.
104. Fournier, R. and R. Potter, Magnesium correction to the Na-K-Ca chemical geothermometer. *Geochimica et Cosmochimica Acta*, 1979. 43(9): p. 1543-1550.
105. Orville, P.M., Alkali ion exchange between vapor and feldspar phases. *American Journal of Science*, 1963. 261(3): p. 201-237.
106. Hemley, J. Aqueous Na/K ratios in the system K₂O-Na₂O-Al₂O₃-SiO₂-H₂O. in *Program, 1967 Ann. Meeting Geol. Soc. Amer. New Orleans*. 1967.
107. Arnorsson, S., Chemical equilibria in Icelandic geothermal systems—implications for chemical geothermometry investigations. *Geothermics*, 1983. 12(2-3): p. 119-128.
108. Kharaka, Y.K. and R.H. Mariner, Chemical geothermometers and their application to formation waters from sedimentary basins, in *Thermal history of sedimentary basins*. 1989, Springer. p. 99-117.
109. Yoshida, Y., Geochemistry of the Nigorikawa geothermal system, southwest Hokkaido, Japan. *Geochemical Journal*, 1991. 25(4): p. 203-222.
110. Larter, S., et al., The controls on the composition of biodegraded oils in the deep subsurface—part 1: biodegradation rates in petroleum reservoirs. *Organic Geochemistry*, 2003. 34(4): p. 601-613.
111. Fournier, R. and A. Truesdell, An empirical Na-K-Ca geothermometer for natural waters. *Geochimica et Cosmochimica Acta*, 1973. 37(5): p. 1255-1275.
112. d'Amore, F., R. Fancelli, and R. Caboi, Observations on the application of chemical geothermometers to some hydrothermal systems in Sardinia. *Geothermics*, 1987. 16(3): p. 271-282.
113. Haiyan, Z., et al., Occurrence and evolution of the Xiaotangshan hot spring in Beijing, China. *Environmental geology*, 2008. 53(7): p. 1483-1489.